decreasing their transcription. Furthermore, total protein levels of these chaperones were essentially unchanged in cells transfected with PLP1msd-FLAG (Fig. 2, *B* and *C*). These results indicate that PDI, CALR, and GRP78 depletion in the ER is not due to a reduction in the total proteins.

Next, we considered the possibility that PLP1msd affected subcellular localization of the ER chaperones from the ER to another cellular compartment. To test this possibility, transfected cells were treated with 0.01% digitonin, which permeabilizes the plasma membrane but not organelles' membranes, followed by treatment with 0.1% SDS, 1% Triton X-100, which permeabilizes the organelles, including the ER (Fig. 2, *D–F*). In cells expressing PLP1msd, the proportion of PDI, CALR, and GRP78 in the fraction containing the plasma membrane and cytosol (soluble fraction) was higher than in cells expressing PLP1wt (Fig. 2, *D* and *E*). In contrast, the amount of these chaperones was lower in fractions containing the ER (insoluble fraction) in PLP1msd expressing cells (Fig. 2, *D* and *F*). Interestingly, the amount of CANX was unchanged in the digitonin-soluble and -insoluble fractions. These results suggest that the decrease in PDI, CALR, and GRP78 in the ER may be due to their translocation from the ER to the plasma membrane or cytosol, but not due to the decrease of total protein.

Recently, Zhang *et al.* (29) reported that ER stress actively promotes GRP78 localization on the cell surface. We confirmed that thapsigargin, a well known ER stressor, increases cell surface expression of PDI in HeLa cells by immunocytochemistry (Fig. 3*A*) and increases cell surface expression of GRP78 and PDI in HeLa cells by cell surface biotinylation (Fig. 3*C*). However, we observed no expression of PDI on the cell surface of PLP1msd-transfected cells (Fig. 3*B*) or no increment of the biotinylated PDI, CALR, and GRP78 in these cells (Fig. 3*D*). These findings suggest that these mutant proteins induce translocation of the chaperones from the ER to the cytosol, rather to the cell surface.

We speculated that mislocalized cytoplasmic chaperons are degraded through a ubiquitin-dependent ERAD pathway. However, although the amounts of ubiquitinated proteins increased in the presence of proteasome inhibitors, MG-132 or lactacystin (Fig. 3*F*), those of the ER chaperons were not affected (Fig. 3*E*), suggesting that they are not degraded through the ERAD pathway after releasing to the cytosol.

Differences and Similarities among Disease-causing Mutations in Other Myelin Genes—To determine whether the depletion of chaperone proteins from the ER is unique to the mutant PLP1 protein or is a common phenomenon observed with mutant proteins encoded by other disease-causing genes, we also examined *PMP22* and *MPZ* genes. Mutations in these genes cause a spectrum of autosomal dominant peripheral demyelinating neuropathies (30).

First, to determine whether accumulation of misfolded proteins in the ER is sufficient to reduce ER chaperone proteins to undetectable levels (by immunostaining) in HeLa cells, we examined two representative PMP22 mutants, *Trembler-J* (*Tr-J*) (an L16P substitution) and *Trembler* (*Tr*) (a G150D substitution), both of which accumulate in the ER by associating with CANX, however, do not induce UPR (31). Both of *Tr-J* and *Tr* are found in humans (32, 33) and mice (34, 35). First, we found no increase in the immunoreactivity of CHOP, which is one of the universal markers of ER stress (36), in either Tr or Tr-j, confirming that these mutants evoked no ER stress (Fig. 4*B*). We then performed immunocytochemistry with the anti-PDI (Fig. 4, *A* and *C*), anti-CALR, and anti-GRP78 (CALR, GRP78, data not shown) antibodies in HeLa cells transfected with the PMP22wt or mutant PMP22 genes. In contrast to our findings in cells transfected with the mutant PLP1 gene, we observed no depletion of these chaperones from the ER in cells expressing the mutant PMP22. These findings indicate that ER accumulation of these mutant proteins, which trigger no ER stress, is insufficient to induce depletion of ER chaperones from the ER.

Next, to analyze whether mutations in another gene that triggers ER stress also deplete the chaperones from the ER, we performed the same experiments using an *MPZ* gene harboring the 506delT mutation (MPZ506delT), which induces ER stress and causes a more severe form of peripheral neuropathy, Dejerine-Sottas neuropathy. This frameshift mutation results in 82 residues of shifted amino acid sequence starting from codon 169 in the MPZ protein (20). CHOP immunofluorescence was increased in the nucleus of HeLa cells transfected with the MPZ506delT gene, but not in cells transfected with the wild-type MPZ gene (MPZwt) (Fig. 4*E*), confirming that this mutant protein is an ER stressor. Immunocytochemistry (Fig. 4*D*) showed that the MPZ506delT mutant, but not MPZwt, increased the number of cells unstained with anti-PDI antibody (Fig. 4*F*). These results strongly suggested that depletion of the chaperones from the ER is not induced solely by protein accumulation in the ER, but instead requires both the accumulation of particular mutant proteins and ER stress. In addition, mutations in disease-causing genes other than *PLP1* can elicit the chaperone depletion.

Depletion of PDI, CALR, and GRP78 Is Linked to PMD Severity—Because ER chaperones are connected with protein folding in the ER, we hypothesized that depletion of the ER chaperones may affect the pathogenesis or severity of PMD. We employed two PLP1 mutants, W163I (11) and I187T (18), both of which result in the mild end of the clinical spectrum of PMD (Fig. 5*A*). Densitometric analysis of CHOP immunofluorescence in transfected HeLa cells confirmed that these milder PLP1 mutants activated the UPR, but to a lesser extent than cells transfected with the PLP1msd gene (Fig. 5*B*).

Next, to analyze whether ER chaperone depletion is associated with clinical severity, we compared the expression of PDI in HeLa cells transfected with these PLP1 mutant genes. We found that the proportion of PDI-unstained cells expressing FLAG-tagged PLP1-W163L or PLP1-I187T was significantly lower than that of cells expressing PLP1msd (Fig. 5*C*). In addition, we observed a similar tendency in cells expressing the MPZ mutants. A mild MPZ allele, MPZS63del, evoked less ER stress and resulted in a smaller proportion of "PDI-unstained cells" than a severe allele, MPZ506delT (data not shown). Together, these results strongly suggest a potential linkage between chaperone depletion and the phenotypic variation in ER stress-related disorders.

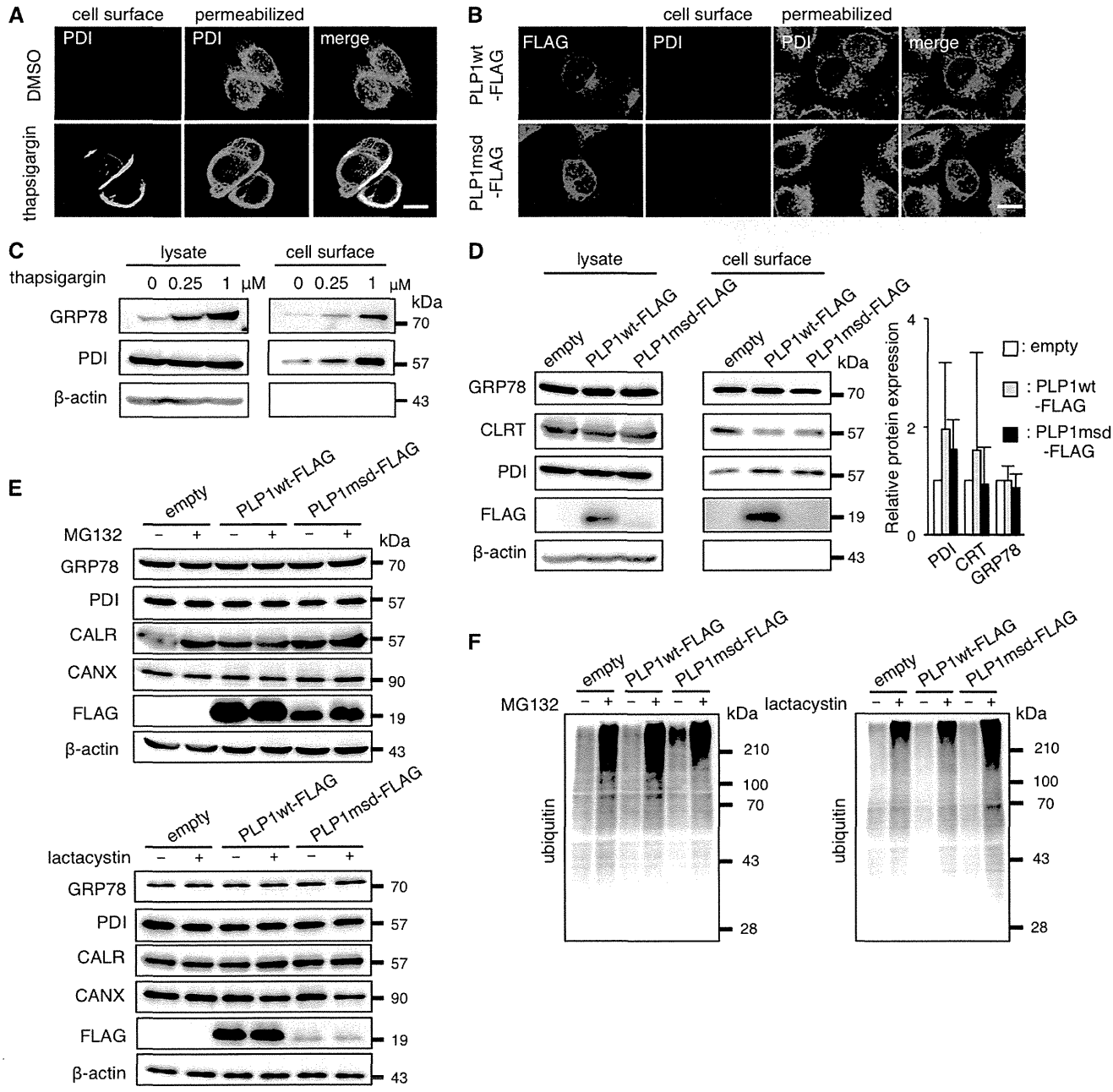

FIGURE 3. **PLP1msd does not increase cell surface expression of the ER chaperones.** *A* and *B*, immunocytochemical analysis of cell surface PDI on HeLa cells treated with 1 μM thapsigargin (*A*) or transfected with the PLP1msd gene (*B*). Cell surface PDI (*green*) were stained with the anti-PDI antibody without permeabilization followed by intracellular staining with the same antibody (*magenta*). *Scale bar*, 10 μm. *C* and *D*, biochemical analysis of cell surface expression of the ER chaperones. HeLa cells were treated with thapsigargin for 16 h (*C*). Transfection was performed before 24 h of cell surface biotinylation (*D*). Cell surface proteins were labeled with biotin, precipitated with streptavidin beads followed by immunoblotting with anti-PDI, anti-CALR, and anti-GRP78 antibodies. *E* and *F*, protease inhibitors do not increase total amounts of the ER chaperones in HeLa cells expressing PLP1msd. Transfected cells were treated with 5 μM MG132 for 16 h or 1 μM lactacystin for 8 h followed by immunoblotting with the anti-PDI, anti-CALR, anti-GRP78, anti-CANX (*E*) and anti-ubiquitin antibodies (*F*). Protein amounts were measured by densitometry. The results are represented as fold-induction against the control experiment using the empty vector. Values are represented as the mean ± S.E. from three independent experiments (*D*).

Down-regulation of Pdi in the SC and Primary Culture of msd Mice—In our *in vitro* analyses, expression of the PDI, CALR, and GRP78 proteins did not increase in cells expressing PLP1msd, despite the significant increase in their transcripts (Fig. 2*A*). To determine whether this also occurs *in vivo*, we further investigated the mRNA and protein expression of these ER chaperones in the SCs isolated from male *msd* mice, which carry the *Plp1A243V* allele, on P14, when the *Plp1* gene is most strongly expressed in the SCs of mutant mice (8). Expression of the *Chop* transcript was significantly higher in *msd* mice than in wild-type mice, suggesting that cells in the SCs of *msd* mice were under ER stress (Fig. 6*A*). We then analyzed the expression of these ER chaperone mRNA by quantitative RT-PCR (Fig. 6*B*). The expression of *Grp78* mRNA was significantly

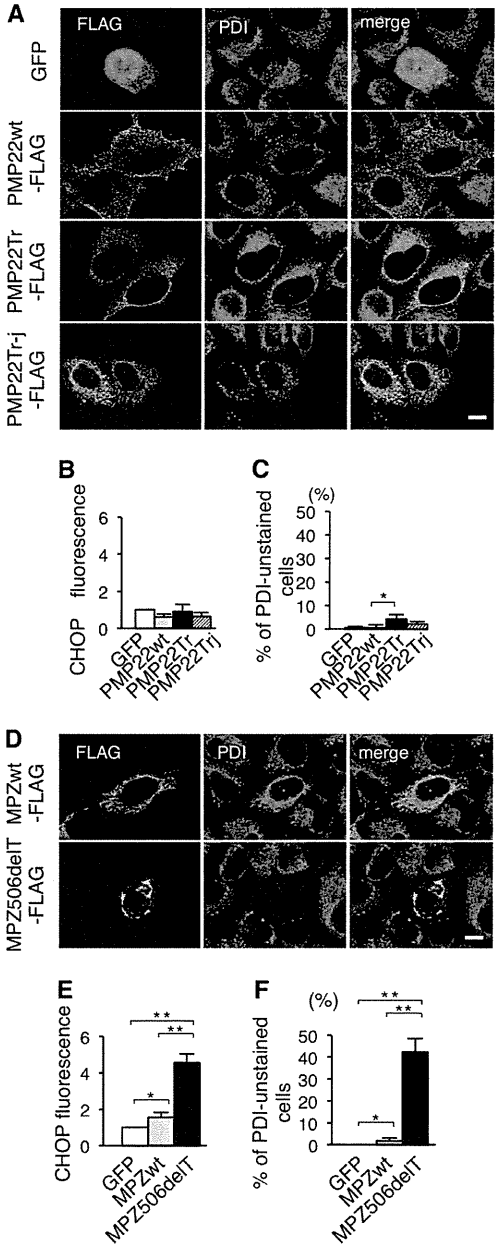

FIGURE 4. **Effect of PMP22 and MPZ mutations on ER chaperones.** *A* and *D*, immunocytochemistry of PDI in HeLa cells transfected with the PMP22wt and mutant PMP22 genes (*A*) or the MPZwt and MPZ506delT genes (*D*). HeLa cells transfected with the indicated vectors were immunostained with the anti-FLAG (*green*) and anti-PDI (*magenta*) antibodies followed by observation with a confocal fluorescence microscope. Note that cells expressing MPZ506delT showed a extremely faint staining pattern for PDI (*arrowhead*). *Scale bar*, 10 μm. *B* and *E*, relative expression of CHOP in HeLa cells transfected with the PMP22wt and mutant PMP22 genes (*B*) or the MPZwt and MPZ506delT genes (*E*). HeLa cells transfected with the indicated vectors were stained with the anti-FLAG and anti-CHOP antibodies together with DAPI to visualize the nuclei. The relative fluorescence intensity of CHOP in the nuclei was analyzed by densitometry. *C* and *F*, proportion of unstained cells with anti-PDI antibody in HeLa cells transfected with the PMP22wt and mutant PMP22 genes (*C*) or the MPZwt and MPZ506delT genes (*F*). Bar graphs are represented as fold-induction ± S.E. against the mean of control experiment from three independent experiments with >100 cells counted in each experiment (*, $p \leq 0.05$; **, $p \leq 0.005$).

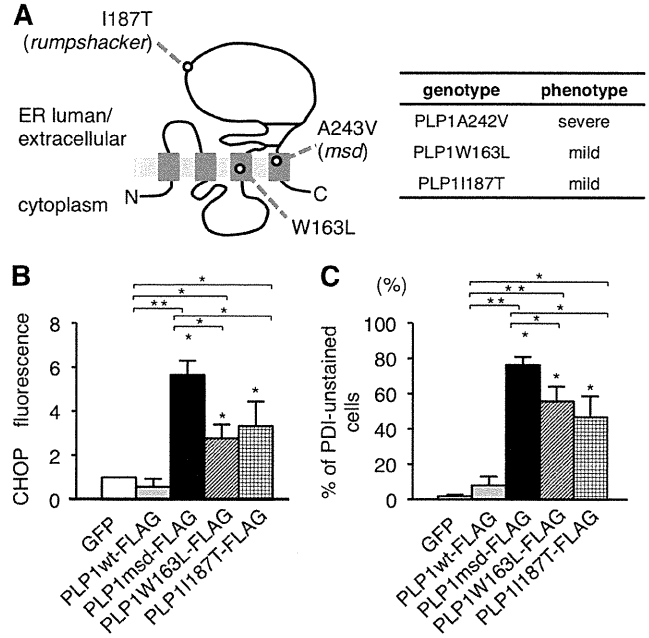

genotype	phenotype
PLP1A242V	severe
PLP1W163L	mild
PLP1I187T	mild

FIGURE 5. **Effect of different PLP1 mutations on ER chaperones.** *A*, schematic diagram of PLP1 with the positions of mutations examined in this study (*left*) and their associated phenotypes (*right*). *B*, expression of CHOP in HeLa cells transfected with the PLP1wt and mutant PLP1 genes. The fluorescence intensity of CHOP in the nuclei was analyzed by densitometry as described in the legend to Fig. 4*B*. *C*, proportion of unstained cells with anti-PDI antibody in HeLa cells transfected with PLP1wt and the indicated PLP1 mutant genes as described in the legend to Fig. 4*C*. Bar graphs are represented as fold-induction ± S.E. against the mean of control experiment from three independent experiments with >100 cells counted in each experiment (*, $p \leq 0.05$; **, $p \leq 0.005$).

increased (2-fold) in *msd* mice. *Pdi* and *Calr* were also up-regulated, but to a lesser extent. However, at protein levels, we observed discordance (Fig. 6, *C* and *D*). Pdi protein expression in *msd* mice was significantly decreased. The expression of Calr showed a similar tendency, although these results did not reach significance ($p = 0.06$). In contrast, Grp78 and Canx protein expression did not differ significantly when compared with wild-type mice.

We also immunocytochemically examined primary MGCs isolated from the brains of embryonic day (E) 14.5 wild-type or *msd* mice. On the 4th day after induction of oligodendrocyte differentiation, profound maturation with increased MBP immunoreactivity was evident in the wild-type MGCs (Fig. 6*E*). In contrast, rapid regression of Oligo2-positive cells and decreased MBP immunoreactivity were observed in the *msd* MGCs, suggesting that oligodendrocyte maturation induced apoptosis in *msd* on the 4th day after induction. Pdi was detected in the cell body of Plp1-positive mature oligodendrocytes in wild-type MGCs, whereas, it was only faintly stained in Plp1-positive oligodendrocytes in the *msd* MGCs. (Fig. 6*F*). These results suggest that endogenous PLP1msd depletes Pdi from the ER of the oligodendrocytes.

Inhibition of GA to ER Transport Is Associated with the Disappearance of PDI, CALR, and GRP78—To determine the underlying mechanism for PDI, CALR, and GRP78 depletion from the ER in cells expressing PLP1 mutants, we further analyzed the effects of the following chemical ER stressors on the

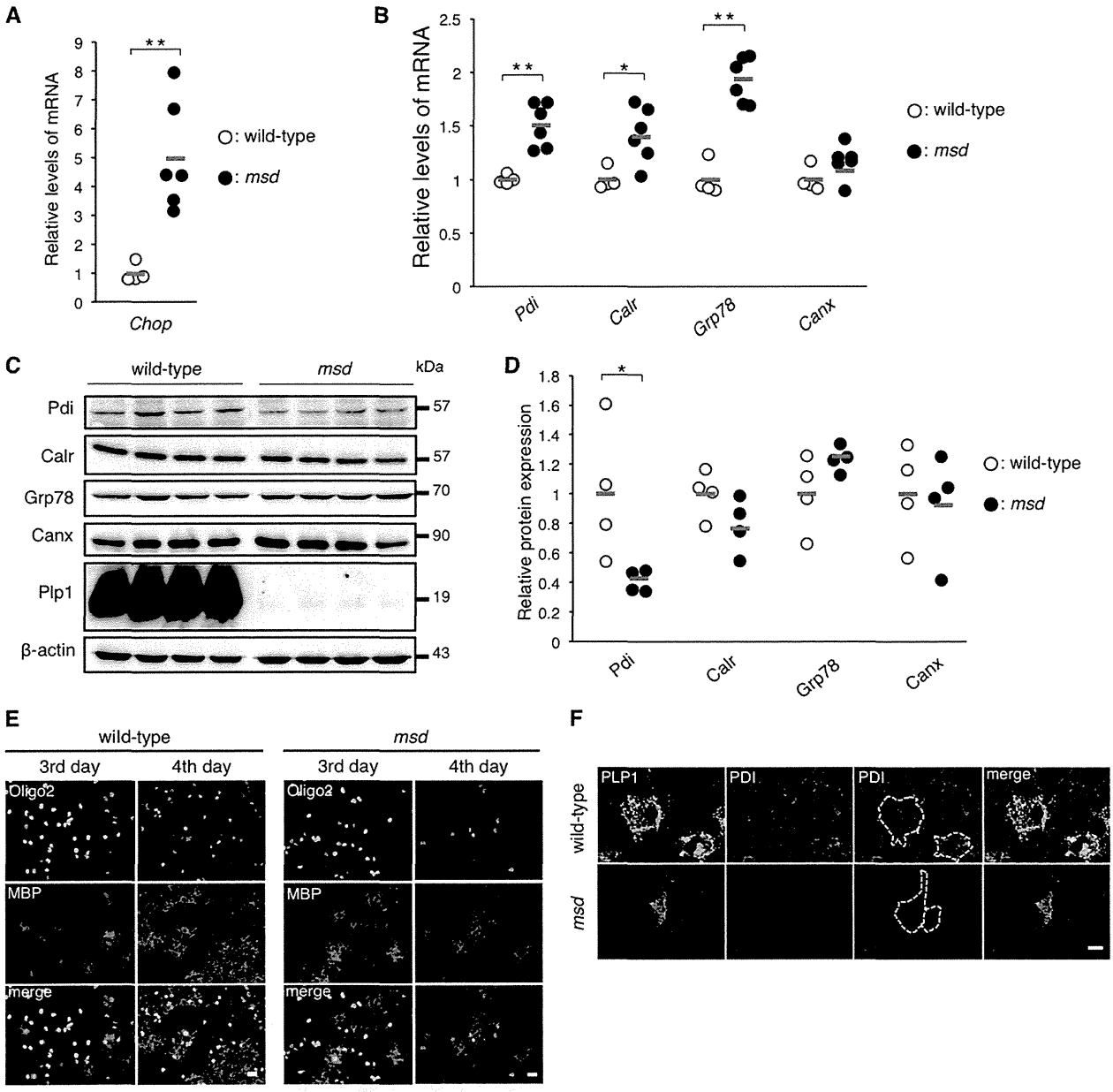

FIGURE 6. **PDI is down-regulated in the SCs and primary oligodendrocytes of *msd* mice.** *A* and *B*, quantitative analysis of *Chop* (*A*), *Pdi*, *Calr*, *Grp78*, and *Canx* genes (*B*) in the SCs of *msd* mice. Quantitative RT-PCR was performed to analyze the expression levels of *Pdi*, *Calr*, *Grp78*, and *Canx* in the SCs of wild-type (*open circle*, $n = 4$) and *msd* (*filled circle*, $n = 6$) mice at P14. *GAPDH* was used as an internal control. The results are represented as fold-induction against the means of wild-type mice. *Red horizontal bars* indicate the mean. *C* and *D*, relative amounts of ER chaperones in the SCs of *msd* mice. The SCs of P14 wild-type (*open circle*, $n = 4$) and *msd* (*filled circle*, $n = 4$) mice were subjected to immunoblotting with the indicated antibodies (*C*). The amounts of the proteins were measured by densitometry and normalized to β-actin (*D*). *E*, expression of MBP and Olig2 in primary oligodendrocytes from *msd* mice. Immunocytochemistry of MBP and Oligo2 in primary oligodendrocytes of *msd* mice. Primary mixed glial cultures were prepared from the forebrains of E14.5 wild-type or *msd* mice. On the 3rd and 4th days after induction of oligodendrocyte differentiation, the oligodendrocytes were immunostained with anti-MBP (*magenta*) and anti-Oligo2 (*green*) antibodies and observed with a confocal fluorescence microscope. *Scale bar*, 5 μm. *F*, immunocytochemistry of PDI in primary oligodendrocytes of *msd* mice. Primary oligodendrocytes prepared from the forebrains of wild-type or *msd* mice at E14.5 and immunostained with anti-PLP1 (*green*) and anti-PDI (*magenta*) antibodies and observed with a confocal microscope. *Scale bar*, 5 μm. *A*, *B*, and *D*, *, $p \leq 0.05$; **, $p \leq 0.005$.

expression of ER chaperones: thapsigargin, a sarco/endoplasmic reticulum Ca^{2+}-ATPase inhibitor; tunicamycin, an *N*-glycosylation inhibitor, and brefeldin A (BFA), a GA-ER transport inhibitor. These three compounds greatly up-regulated the transcripts of *CHOP* and *GRP78*, confirming that they work as ER stressors (Figs. 7, *B* and *C*, and 8, *B*, *C*, *E*, and *F*). These compounds also slightly but significantly increased the expression of *PDI*, *CALR*, and *CANX* transcripts.

Next, HeLa cells were treated with these compounds for 8 h, followed by immunocytochemistry with anti-PDI, anti-CALR, anti-GRP78, or anti-CANX antibodies. Thapsigargin and tunicamycin did not alter the expression of the chaperones (Fig. 8*A*), even after an extended incubation (Fig. 8*D*). In contrast, BFA treatment clearly diminished PDI, CALR, and GRP78 from the ER; however, CANX expression remained unchanged (Fig. 7*A*). In BFA-treated HeLa cells, total amounts of the chaperone

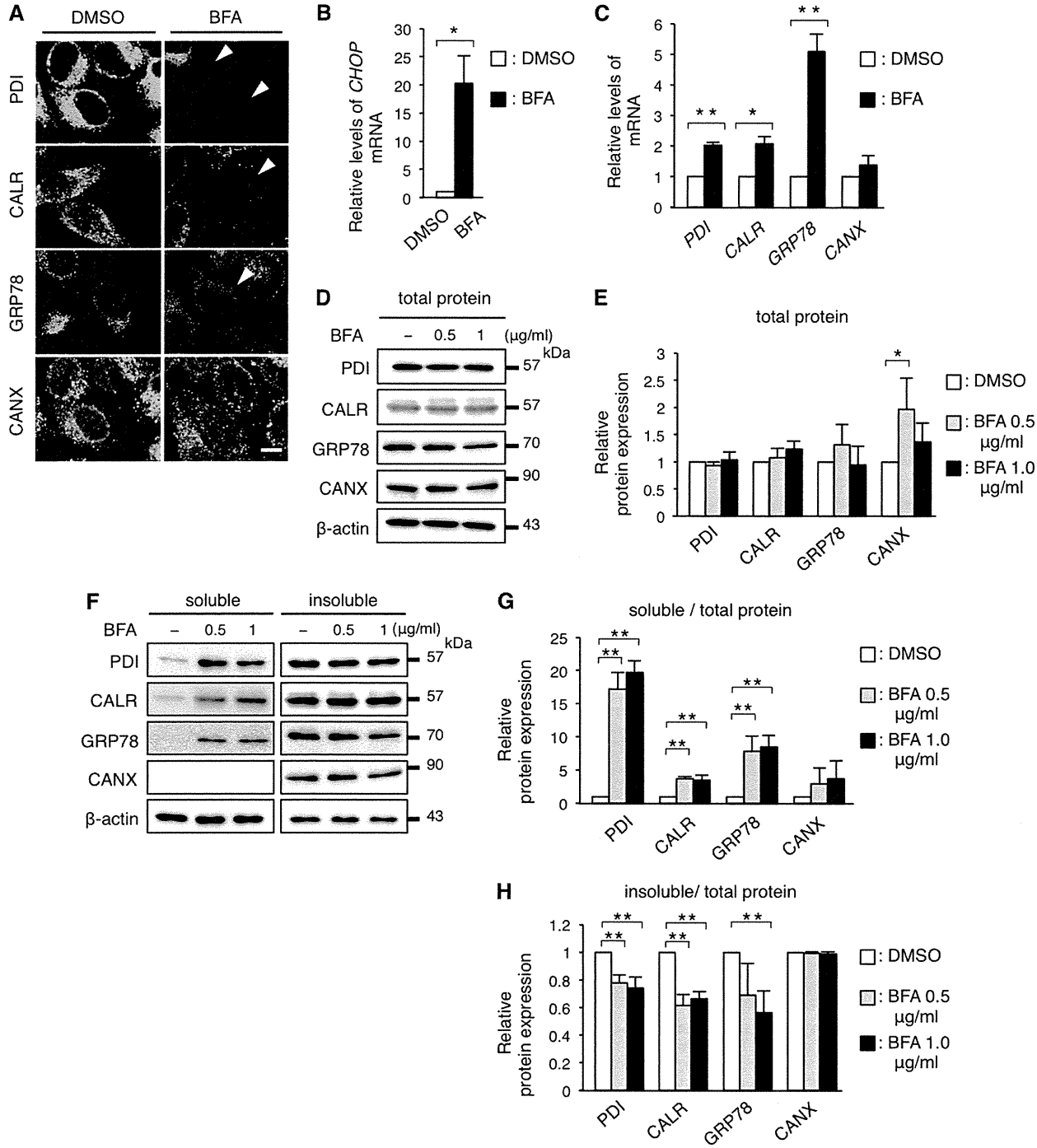

FIGURE 7. **BFA treatment recapitulates the disappearance of PDI, CALR, and GRP78.** *A*, immunocytochemistry of ER chaperones in HeLa cells treated with BFA. HeLa cells were treated with 1 μg/ml of BFA for 8 h were immunostained with the indicated antibodies and observed with a confocal fluorescence microscope. *Scale bar*, 10 μm. Note that cells treated with BFA showed extremely faint staining (*arrowheads*) for PDI, CALR, and GRP78. *B* and *C*, relative expression of the transcripts of the ER chaperones in HeLa cells treated with BFA. Expression levels of the transcripts of *CHOP* (B), *PDI*, *CALR*, *GRP78*, and *CANX* mRNA (*C*) in HeLa cells treated with BFA were analyzed by qRT-PCR and normalized to *GAPDH*. *D* and *E*, total amounts of PDI, CALR, GRP78, and CANX in HeLa cells treated with BFA. HeLa cells were treated with BFA as in *A* and subjected to immunoblotting with the indicated antibodies (*D*). The amounts of the proteins were measured by densitometry and normalized to β-actin (*E*). *F-H*, digitonin fractionation of HeLa cells treated with BFA. Digitonin fractionation was performed as described in the legend to Fig. 2*D* and the extracts were subjected to immunoblotting with the indicated antibodies (*F*) followed by quantitative analysis (*G* and *H*) as in Fig. 2, *E* and *F*. Results are represented as fold-induction compared with DMSO control experiment. Values are represented as the mean ± S.E. from three independent experiments (*, $p \leq 0.05$, **, $p \leq 0.005$).

proteins (except for CANX at 0.5 μg/ml of BFA treatment) were mostly unaffected despite their increased transcripts (Fig. 7, *D* and *E*), as was observed in HeLa cells transfected with the PLP1msd gene (Fig. 2, *B* and *C*). We performed fractionation experiments with 0.01% digitonin as described in Fig. 2*D*. In the BFA-treated HeLa cells, the proportion of PDI, CALR, and

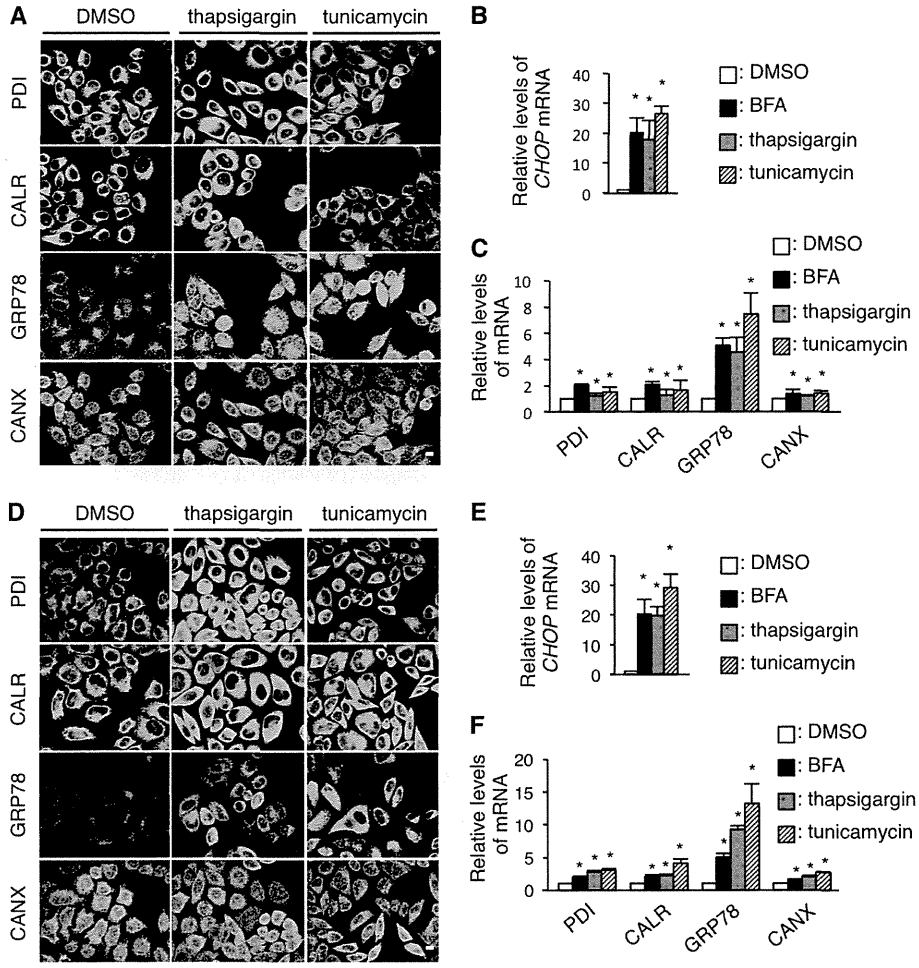

FIGURE 8. **Thapsigargin and tunicamycin treatments do not cause the depletion of PDI, CALR, and GRP78.** *A* and *D*, immunocytochemistry of ER chaperones in HeLa cells treated with thapsigargin and tunicamycin. HeLa cells were treated with 1 μM thapsigargin or 2 μM tunicamycin for 8 (*A*) or 24 h (*D*), immunostained with the indicated antibodies and observed with a confocal fluorescence microscope. *Scale bar*, 5 μm. *B*, *C*, *E*, and *F*, quantitative RT-PCR for *CHOP* (*B* and *E*) *PDI*, *CALR*, *GRP78*, and *CANX* (*C* and *F*) genes in HeLa cells treated with 1 μM thapsigargin or 2 μM tunicamycin for 8 h (*B* and *C*) or 24 h (*E* and *F*). The *GAPDH* gene was used as an internal control. Results are represented as fold-induction compared with DMSO control experiment. Values are represented as the mean ± S.E. from three independent experiments (*, $p \leq 0.05$; **, $p \leq 0.005$).

GRP78 in the digitonin-soluble fraction containing the cytosol and plasma membrane was significantly higher, whereas the proportion of these proteins in the insoluble fraction containing ER proteins was lower than in untreated cells (Fig. 7, *F–H*); similar to that observed in cells expressing the mutant PLP1 (Fig. 2, *D–F*). This multitude of common evidence between BFA-treated and PLP1msd-transfected cells suggests that these may have a common mechanism underlying depletion of PDI, CALR, and GRP78.

The Fragmentation of GA in Cells Expressing PLP1msd and Phenotypically Milder PLP1 Mutants—As previously reported (37), BFA induces fragmentation of the GA (Fig. 9*A*). To further examine whether the mutant proteins affect the structure of the GA, we co-transfected GFP vector and the PLP1msd gene in HeLa cells and immunostained cells with antibodies against GM130, a GA marker, and PDI. We found that the GA was fragmented in GFP^+ cells, which are expressing PLP1msd (Fig. 9*B*). These cells were not stained with anti-PDI antibody. This GA fragmentation was not observed in cells expressing PLP1wt. GM130 co-localized with the dense signal of PLP1wt at the perinuclear structure, presumably staining normal GA. We also found that expression of the *MPZ506delT* mutation also induced fragmentation of the GA in HeLa cells, whereas MPZwt, PMP22wt, and both Tr and Tr-j PMP22 mutants did not induce any morphological changes of the GA (Fig. 9*C*). These findings suggest that ER stressor proteins also induce GA fragmentation.

Next, to determine whether fragmentation of the GA is associated with the phenotypic variation in PMD patients, we evaluated the GA structure in HeLa cells transfected with the PLP1msd and two milder PLP1 mutants and classified the GA morphology into three categories, "normal," "mild fragmentation," and "severe fragmentation," as previously reported elsewhere (38). Cells expressing each mild allele showed a higher proportion of "severe" GA fragmentation than those expressing PLP1wt; however, this proportion was lower than in cells expressing PLP1msd (Fig. 9*D*). These results suggest that GA fragmentation is involved in pathogenesis of disease-causing PLP1 mutations, and that the degree of GA fragmentation is associated with the severity of PMD, in conjunction with depletion of the ER chaperones.

Depletion of ER Chaperones and GA Fragmentation in PMD

Obstruction of Membrane and Secretory Protein Transport by PLP1msd—Newly synthesized membrane and secretory proteins are transported from the ER to the GA when they undergo post-translational modification (39). ER chaperone proteins are subsequently transported back to the ER from the *cis*-Golgi. In contrast, other membrane and secretory proteins that reach the *trans*-Golgi are sorted to carriers for further transport to various cellular destinations (40) (Fig. 10*A*). We hypothesized that PLP1msd interferes with the maturation of these proteins because it depletes the ER chaperones, which assist with protein folding in the ER, and induces morphological changes in the GA. To test this hypothesis, we created an expression vector encoding membrane-linked cell surface GFP, summarized in Fig. 9*E*. When HeLa cells were co-transfected with either PLP1wt-FLAG or PLP1msd-FLAG along with the cell surface GFP, we found that expression of the reporter protein was mis-

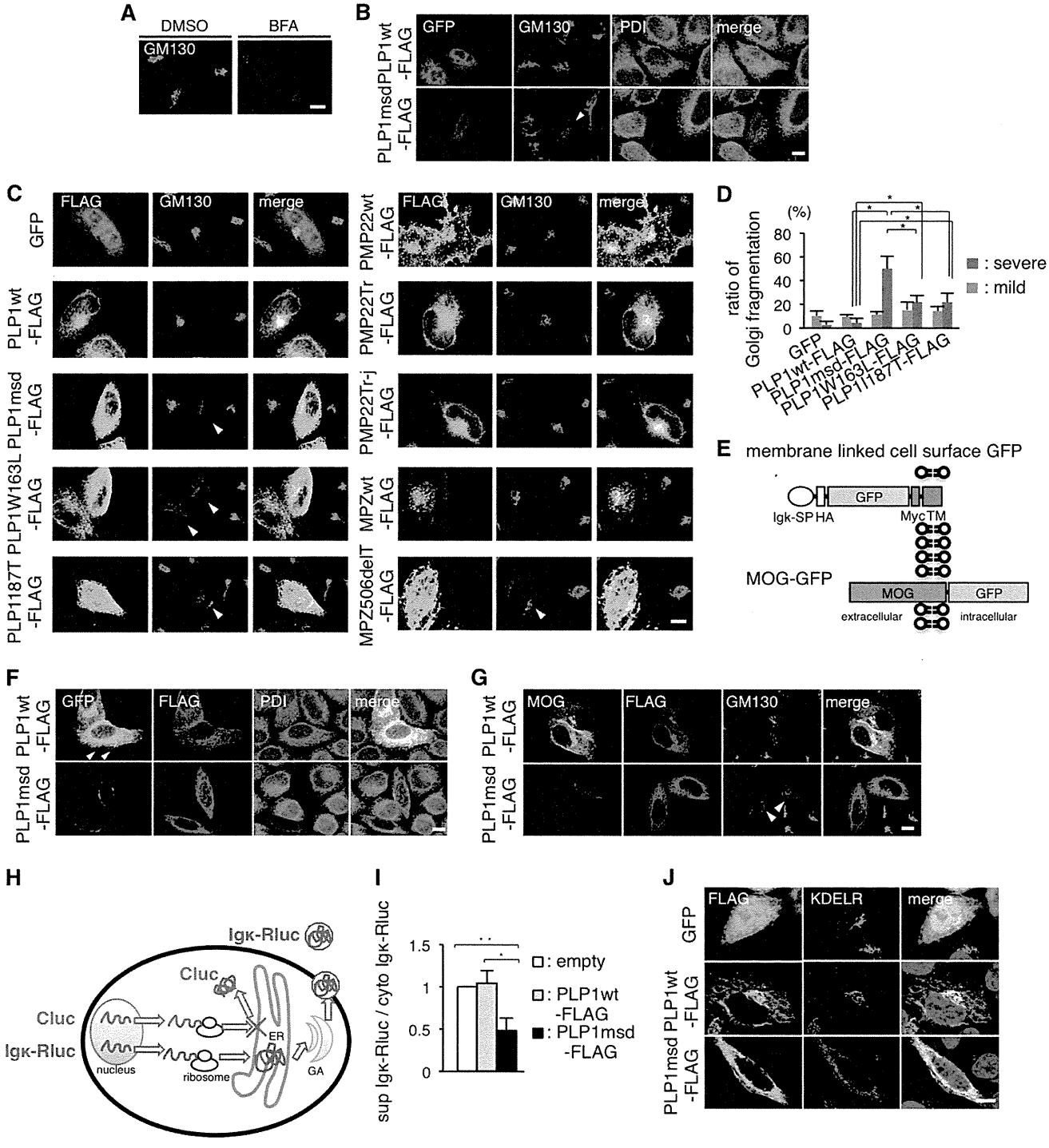

localized in cells co-transfected with the PLP1msd gene (Fig. 9*F*). On the other hand, co-transfection with the PLP1wt gene showed GFP fluorescence in the cell surface. Such phenomenon was also observed in HeLa cells co-transfected with the *MOG* gene (41), which is an oligodendrocyte-specific membrane protein, fused with the GFP gene (MOG-GFP, summarized in Fig. 9, *E* and *G*). These findings suggested the possibility that PLP1msd impairs the transport of membrane proteins from the ER to the cell surface through the GA.

Furthermore, we analyzed whether intracellular transport of the secretory proteins was also affected by PLP1msd. We created a reporter secretory protein, in which *Renilla* luciferase (Rluc) was fused at the N terminus with the signal sequence of Igκ light chain (Igκ-Rluc). This fusion protein penetrates into the ER and is secreted to the extracellular space through the GA. HeLa cells were co-transfected with the regular firefly luciferase (cytoplasmic luciferase, Cluc) gene and the Igκ-Rluc gene along with an empty vector, PLP1wt-FLAG or PLP1msd-FLAG gene (Fig. 9*H*). We then simultaneously measured Cluc and Igκ-Rluc in cell lysate and culture supernatants with a luminometer. Total Rluc activity normalized to Cluc activity did not differ among cells expressing empty vector, PLP1wt, and PLP1msd, confirming a stable translation ratio between ER-mediated and non-ER-mediated processes (data not shown). Of note, we found that expression of the Igκ-Rluc protein in the culture supernatant normalized to intracellular Igκ-Rluc was significantly lower in cells transfected with the PLP1msd gene (Fig. 9*I*). Immunocytochemistry revealed that the Igκ-Rluc reporter protein is faintly localized in the GA in cells expressing PLP1wt; whereas, the same protein is clearly accumulated in the ER of cells expressing PLP1msd (data not shown). Together, these results suggest that PLP1msd induces obstruction of membrane and secretory protein transport.

PLP1msd Disturbs the Localization of KDEL Receptor in the GA—PDI, CALR, and GRP78 contain a carboxyl-terminal retrieval signal KDEL (Lys-Asp-Glu-Leu) motif (42). The KDEL motif is recognized by the KDEL receptor in the GA after releasing the chaperones from the ER, and then the chaperones are retrogradely transported back to the ER by the receptor in a coatomer protein I-dependent manner (43) (Fig. 10*A*). In contrast, CANX, which lacks a KDEL motif, was not depleted by PLP1msd transfection. These results promote us to investigate subcellular localization of the KDEL receptor in cells expressing PLP1msd. The KDEL receptor mainly localizes in the GA (44). Surprisingly, in the PLP1msd-transfected cells, the KDEL receptor was displayed as a mesh-like distribution through the cells and co-localized well with PLP1msd (Fig. 9*J*). In the cells expressing PLP1wt, we observed that the KDEL receptor co-localized with PLP1wt at the perinuclear structure, which was probably localized in the GA as shown in Fig. 9*B*. These results suggest that PLP1msd induced mislocalization of the KDEL receptor.

DISCUSSION

Involvement of ER stress and the subsequent UPR has been implicated in pathogenesis of multiple human inherited diseases, including cystic fibrosis (45), retinitis pigmentosa (46), CMT (22), and PMD (8, 11). Although there is wide phenotypic variation in each of these diseases, even among the mutations in same genes, little is known about the factors that determine the difference in ER stress and the severity of disease. In this study, we investigated the organelle changes in cells expressing different *PLP1* missense mutations associated with a wide-range of clinical severities in PMD. We demonstrated that accumulation of the ER stress-associated mutant PLP1 leads to depletion of some important ER chaperones and GA fragmentation, both of which are more profound in cells expressing mutants associated with more severe phenotypes. We also found that an ER stress-related MPZ mutant also induces these cellular phenotypes; however, two PMP22 mutants, which cannot induce ER stress despite their ER retention, do not induce them. Based on these findings, we suggest that the cellular phenotypes of ER chaperone depletion and GA fragmentation may be involved in

FIGURE 9. **PLP1msd overexpression induces GA fragmentation, retention of MOG in the ER, and reduction of protein secretion.** *A* and *B*, immunocytochemistry of GM130 in HeLa cells treated with BFA (*A*) and HeLa cells expressing PLP1wt or PLP1msd (*B*). HeLa cells were treated with DMSO (as a control) or BFA as described in the legend to Fig. 7*A*. HeLa cells co-transfected with GFP (to visualize transfected cells) along with PLP1wt-FLAG or PLP1msd-FLAG were immunostained using anti-GM130 (*blue*) and anti-PDI (*magenta*) antibodies and were observed with a confocal fluorescence microscope. Cells expressing PLP1msd showed the fragmentation of the GA (*arrowhead*). *Scale bar*, 10 μm. *C*, immunocytochemistry of GM130 in HeLa cells expressing PLP1, PMP22, and MPZ mutants. HeLa cells transfected with the indicated vectors were immunostained with the anti-FLAG (*green*) and anti-GM130 (*magenta*) antibodies. Note that cells expressing PLP1 mutants and MPZ506delT showed fragmentation of GA detected by GM130 staining (*arrowheads*). *Scale bar*, 10 μm. *D*, the proportion of cells showing GA fragmentation in HeLa cells transfected with PLP1wt or mutant PLP1 genes, as shown in *B* and *C*. FLAG-positive cells were classified into 3 categories based on GA morphology, as normal, mild fragmentation, and severe fragmentation and the number of cells in each class was counted. Data for normal are not shown. The results are represented as the mean ± S.E. from three independent experiments with >100 cells counted in each experiment (*, $p \leq 0.05$; **, $p \leq 0.005$). *E*, scheme for the construction of membrane-linked cell surface GFP and MOG-GFP. *SP*, signal peptide; *Igκ*, immunoglobulin κ light chain; *HA*, hemagglutinin; *TM*, transmembrane of platelet-derived growth factor receptor. *F* and *G*, subcellular localization of membrane-linked cell surface GFP (*F*) or MOG-GFP (*G*) in HeLa cells expressing PLP1wt-FLAG or PLP1msd-FLAG. HeLa cells co-transfected with membrane-linked cell surface GFP or MOG-GFP along with PLP1wt-FLAG or PLP1msd-FLAG were immunostained using anti-FLAG (*blue*) and anti-PDI (*magenta*) antibodies. Cells expressing PLP1wt showed the cell surface GFP expression (*arrowhead*). *Scale bar*, 10 μm. *H*, scheme for the luciferase reporter assay. Secretary *Renilla* luciferase (Igκ-Rluc, *blue*), which is fused with Igκ signal peptide, penetrates into the ER and is secreted to the extracellular space through the GA. Firefly luciferase (Cluc, *red*), which is a cytosolic protein, served as an internal control. This system enables the measurement of secretion of the secretory reporter protein in live cells by comparing the total and supernatant activities of Igκ-Rluc. Co-transfection with the Cluc gene not only detects leakage of these reporter proteins to the supernatant from dead cells, but also compares translation efficacies between cytoplasmic and secretary proteins. *I*, luciferase reporter assay to evaluate the effect of PLP1msd on the secretory protein transport. HeLa cells were co-transfected with the firefly luciferase (Cluc) and Igκ-Rluc genes along with an empty vector, PLP1wt-FLAG, or PLP1msd-FLAG. Each of Cluc and Igκ-Rluc in the cell lysate and supernatant was simultaneously measured by a luminometer. Efficient of secretion of Igκ-Rluc was calculated as follows: *Renilla* luciferase activity of supernatant/total (supernatant plus cytosol) *Renilla* luciferase activity. Results are represented as fold-induction compared with empty vector control experiment. Values are represented as the mean ± S.E. from three independent experiments (*, $p \leq 0.05$; **, $p \leq 0.005$). *J*, immunocytochemistry of KDEL receptor in HeLa cells expressing PLP1wt or PLP1msd. HeLa cells transfected with the indicated vectors were immunostained with the anti-FLAG (*green*) and anti-KDEL receptor (*magenta*) antibodies and observed with a confocal fluorescence microscope. *Scale bar*, 5 μm.

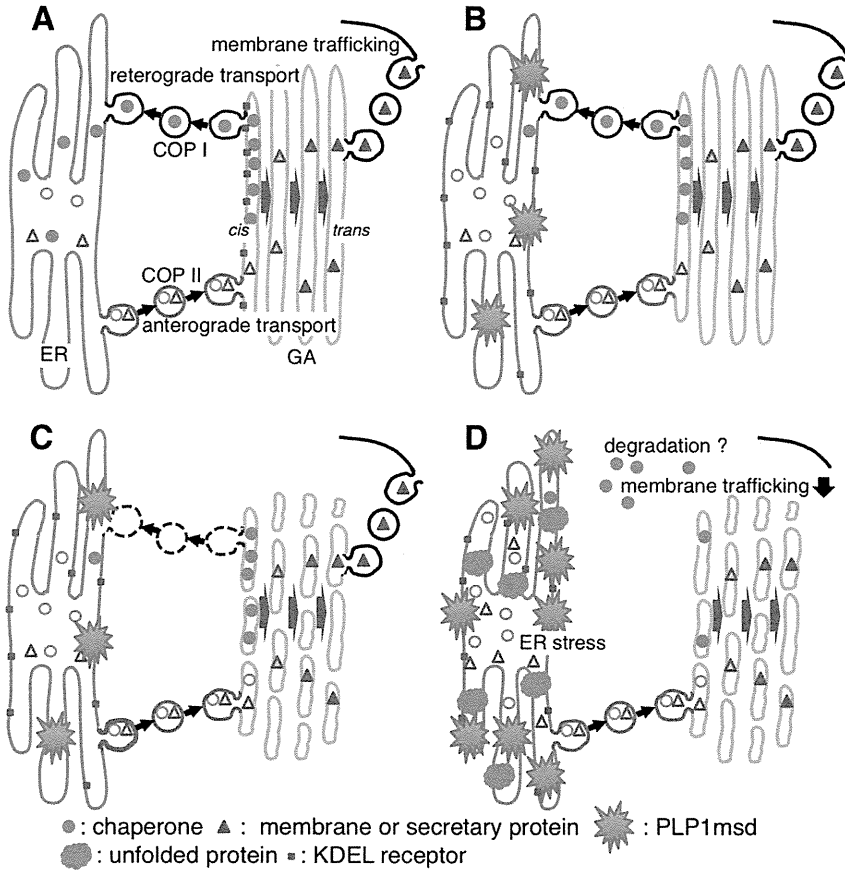

FIGURE 10. **Scheme for the mechanism of ER chaperone depletion and GA fragmentation.** *A*, under physiological conditions, efficient amounts of mature ER chaperones (*filled circles*) can fold unfolded proteins into their correct conformation. Immature ER chaperones with KDEL motifs (*open circles*), along with membrane and secretory proteins (*triangles*), are first transported from ER exit sites to the entry (*cis*) side of the GA to undergo post-translational modifications (coatomer protein (*COPII*) II-mediated anterograde transport). The ER chaperones are recycled back to the ER through the interaction with the KDEL receptor (*red square*) in the GA (coatomer protein I-mediated retrograde transport). In contrast, mature membrane and secretory proteins that reach to the *trans*-Golgi are further transported to various cellular destinations. *B*, ER stress-related mutant protein (*red spines*) induces dysfunction of retrograde transport from the GA to the ER by KDEL receptor mis-localized in the ER, resulting in a reduced supply of ER chaperones. *C*, this inhibition of retrograde transport, and probably the ER stress itself, may lead to the fragmentation of the GA. *D*, dysfunction of the ER to GA transport may jam membrane and secretory protein trafficking, leading to the further accumulation of misfolded proteins (*orange*). These changes in cellular homeostasis triggered by misfolded mutant proteins may further accelerate ER stress.

the pathogenesis of particular mutations in certain genes in ER stress-related diseases.

We observed that PDI, CALR, and GRP78 were depleted in the ER of HeLa cells transfected with the PLP1msd gene, whereas CANX remained unaffected. Similar phenomenon was also observed in endogenous Pdi and Calr in the SCs of *msd* mice (Fig. 6, *C* and *D*). By contrast, we could not find an obvious decrease of endogenous Grp78 in the mutant SCs, possibly due to the large enhancement of mRNA up-regulation. We considered the features that were either functionally or structurally common among the depleted chaperones. Functionally, each of these chaperones has a distinct role in protein folding and maintenance of ER homeostasis. For example, PDI catalyzes the formation and rearrangement of molecular disulfide bonds for protein folding (47). CALR and CANX are calcium-binding proteins implicated in the trimming of *N*-glycosylation and storage of calcium in the ER (48). GRP78 controls activation of the UPR, acting as a sensor for misfolded proteins in the ER (49). Based on this evidence, it is unlikely that the depletion is linked to a particular function of these chaperones.

Structurally, PDI, CALR, and GRP78 contain a carboxyl-terminal retrieval signal KDEL motif (42), which is recognized by the KDEL receptor to transport them back to the ER (43). This retrieval mechanism by the KDEL receptor contributes to quality control at the ER (50). We observed that the KDEL receptor was localized in the ER in cells expressing PLP1msd, whereas the same protein was localized in the GA in PLP1wt and control cells (Fig. 9*J*). Moreover, depletion of PDI, CALR, and GRP78 was also observed in HeLa cells treated with the chemical ER stressor, BFA, which inhibits retrograde transport from the GA to the ER (51, 52). Interestingly, the other chemical ER stressors tested, thapsigargin and tunicamycin, did not recapitulate the findings. These results suggest that misfolded mutant proteins may induce ER chaperone depletion by inhibition of their KDEL receptor-mediated retrograde transport of these chaperones by mis-localizing KDEL receptor.

Our results suggested that PLP1 and MPZ mutants, and possibly other mutant proteins that evoke ER stress, specifically deplete chaperones containing a KDEL motif from the ER. These proteins were unlikely degraded by the ERAD-protea-

some system (Figs. 2, *B* and *C*, and 3, *E* and *F*). We further demonstrated that the proportion of these chaperone proteins in the digitonin-soluble fraction, which contains the plasma membrane and cytosolic proteins, increased in cells expressing PLP1msd (Fig. 2, *D* and *E*). However, we found no change in the amounts of these chaperone proteins on the cell surface (Fig. 3, *B* and *D*). These results suggest that KDEL-containing ER chaperones mainly translocate from the ER to the cytosol in cells expressing ER stress proteins. However, we could not rule out a possibility that small populations may translocate to the plasma membrane, as described previously (29).

In contrast, the GA fragmentation observed in cells treated with BFA was also observed in cells treated with thapsigargin (data not shown). GA fragmentation has been reported in another ER stress-related disorder, ALS (53). These findings suggest that GA fragmentation may be a common pathology in ER stress-related diseases.

An association between cellular pathology and clinical severity for PLP1 mutations has been reported. Gow and Lazzarini (10) reported a cellular mechanism that the amount of mutant *PLP1* gene product accumulated in the ER accounts for disease severity in PMD. Recent studies showed that differences in the UPR (9) and ER quality control (11) have the potential to modulate disease severity. These reports suggest that retention of PLP1 mutants determines the severity of ER stress and clinical outcome. Consistent with these findings, the depletion of ER chaperones and GA fragmentation are closely linked to clinical severity (Figs. 5*C* and 9*D*), indicating that these cellular phenotypes are associated with disease pathology. In addition, we also demonstrated that PLP1msd not only induces ER stress, but also inhibits secretion and cell surface expression of proteins, probably due to impairment of ER chaperone transport from the GA to the ER and/or GA fragmentation. These trafficking defects may also contribute to the pathogenesis of disease by preventing cell-to-cell and cell-to-environment communications. Additional studies are required to elucidate how these mutants affect the maturation and trafficking of other membrane and secretory proteins.

Based on our findings, we propose a novel model for mechanisms to explain how mutant misfolded proteins affect intracellular homeostasis, as summarized in Fig. 10. When misfolded proteins accumulate in the ER, they inhibit GA to ER retrograde transport by KDEL receptor mis-localization in the ER (Fig. 10*B*). Ultimately, inhibition of retrograde transport results in depletion of KDEL-containing ER chaperones from the ER. Blockage of GA to ER retrograde transport also contributes to abnormal accumulation of ER chaperones in the *cis*-Golgi, which may, in part, contribute to GA fragmentation (Fig. 10*C*). As a consequence, the ER to GA transport of membrane/secretory proteins is disturbed, and misfolded proteins and other membrane/secretory proteins accumulate in the ER, resulting in a trafficking defect and further acceleration of ER stress (Fig. 10*D*). This unexpected discovery and new model for the disease mechanism may promote our understanding of how different mutations in the same gene differently evoke ER stress and affect disease phenotype. Our findings may have further implications for ER stress-related diseases in which the UPR modulates pathology. Because practically no effective treatment is available for these diseases, ER chaperone and GA may serve as potential targets for therapeutic intervention.

Acknowledgments—We thank Dr. W. B. Macklin (Cleveland Clinic Foundation) for providing msd mice, Dr. H. Osaka (Kanagawa Children's Medical Center) for the human PLP1 genes, Dr. J. R. Lupski (Baylor College of Medicine) for the human PMP22 genes and MPZ genes, Dr. J. Miyazaki (Osaka University) for pCAGGS, and Dr. M. Itoh (NCNP) for anti-PLP1 antibody, respectively.

REFERENCES

1. Kaufman, R. J. (2002) Orchestrating the unfolded protein response in health and disease. *J. Clin. Invest.* **110,** 1389–1398
2. Lindholm, D., Wootz, H., and Korhonen, L. (2006) ER stress and neurodegenerative diseases. *Cell Death Differ.* **13,** 385–392
3. Szegezdi, E., Logue, S. E., Gorman, A. M., and Samali, A. (2006) Mediators of endoplasmic reticulum stress-induced apoptosis. *EMBO Rep.* **7,** 880–885
4. Yamamoto, K., Sato, T., Matsui, T., Sato, M., Okada, T., Yoshida, H., Harada, A., and Mori, K. (2007) Transcriptional induction of mammalian ER quality control proteins is mediated by single or combined action of ATF6α and XBP1. *Dev. Cell* **13,** 365–376
5. Calfon, M., Zeng, H., Urano, F., Till, J. H., Hubbard, S. R., Harding, H. P., Clark, S. G., and Ron, D. (2002) IRE1 couples endoplasmic reticulum load to secretory capacity by processing the XBP-1 mRNA. *Nature* **415,** 92–96
6. Yoshida, H., Matsui, T., Yamamoto, A., Okada, T., and Mori, K. (2001) XBP1 mRNA is induced by ATF6 and spliced by IRE1 in response to ER stress to produce a highly active transcription factor. *Cell* **107,** 881–891
7. Inoue, K. (2005) PLP1-related inherited dysmyelinating disorders. Pelizaeus-Merzbacher disease and spastic paraplegia type 2. *Neurogenetics* **6,** 1–16
8. Southwood, C. M., Garbern, J., Jiang, W., and Gow, A. (2002) The unfolded protein response modulates disease severity in Pelizaeus-Merzbacher disease. *Neuron* **36,** 585–596
9. Gow, A., Southwood, C. M., and Lazzarini, R. A. (1998) Disrupted proteolipid protein trafficking results in oligodendrocyte apoptosis in an animal model of Pelizaeus-Merzbacher disease. *J. Cell Biol.* **140,** 925–934
10. Gow, A., and Lazzarini, R. A. (1996) A cellular mechanism governing the severity of Pelizaeus-Merzbacher disease. *Nat. Genet.* **13,** 422–428
11. Roboti, P., Swanton, E., and High, S. (2009) Differences in endoplasmic-reticulum quality control determine the cellular response to disease-associated mutants of proteolipid protein. *J. Cell Sci.* **122,** 3942–3953
12. Swanton, E., High, S., and Woodman, P. (2003) Role of calnexin in the glycan-independent quality control of proteolipid protein. *EMBO J.* **22,** 2948–2958
13. Bernard-Marissal, N., Moumen, A., Sunyach, C., Pellegrino, C., Dudley, K., Henderson, C. E., Raoul, C., and Pettmann, B. (2012) Reduced calreticulin levels link endoplasmic reticulum stress and Fas-triggered cell death in motoneurons vulnerable to ALS. *J. Neurosci.* **32,** 4901–4912
14. Jaronen, M., Vehvilainen, P., Malm, T., Keksa-Goldsteine, V., Pollari, E., Valonen, P., Koistinaho, J., and Goldsteins, G. (2012) Protein disulfide isomerase in ALS mouse glia links protein misfolding with NADPH oxidase-catalyzed superoxide production. *Hum. Mol. Genet.* **22,** 646–655
15. Gencic, S., and Hudson, L. D. (1990) Conservative amino acid substitution in the myelin proteolipid protein of jimpy(msd) mice. *J. Neurosci.* **10,** 117–124
16. Yamamoto, T., Nanba, E., Zhang, H., Sasaki, M., Komaki, H., and Takeshita, K. (1998) Jimpy(msd) mouse mutation and connatal Pelizaeus-Merzbacher disease. *Am. J. Med. Genet.* **75,** 439–440
17. Koizume, S., Takizawa, S., Fujita, K., Aida, N., Yamashita, S., Miyagi, Y., and Osaka, H. (2006) Aberrant trafficking of a proteolipid protein in a mild Pelizaeus-Merzbacher disease. *Neuroscience* **141,** 1861–1869
18. Kobayashi, H., Hoffman, E. P., and Marks, H. G. (1994) The rumpshaker mutation in spastic paraplegia. *Nat. Genet.* **7,** 351–352
19. Schneider, A., Montague, P., Griffiths, I., Fanarraga, M., Kennedy, P., Brophy, P., and Nave, K. A. (1992) Uncoupling of hypomyelination and glial cell death by a mutation in the proteolipid protein gene. *Nature* **358,**

758–761
20. Khajavi, M., Inoue, K., Wiszniewski, W., Ohyama, T., Snipes, G. J., and Lupski, J. R. (2005) Curcumin treatment abrogates endoplasmic reticulum retention and aggregation-induced apoptosis associated with neuropathy-causing myelin protein zero-truncating mutants. *Am. J. Hum. Genet.* **77,** 841–850
21. D'Antonio, M., Feltri, M. L., and Wrabetz, L. (2009) Myelin under stress. *J. Neurosci. Res.* **87,** 3241–3249
22. Gow, A., and Sharma, R. (2003) The unfolded protein response in protein aggregating diseases. *Neuromolecular Med.* **4,** 73–94
23. Warner, L. E., Garcia, C. A., and Lupski, J. R. (1999) Hereditary peripheral neuropathies. Clinical forms, genetics, and molecular mechanisms. *Annu. Rev. Med.* **50,** 263–275
24. Yu, L. H., Morimura, T., Numata, Y., Yamamoto, R., Inoue, N., Antalfy, B., Goto, Y., Deguchi, K., Osaka, H., and Inoue, K. (2012) Effect of curcumin in a mouse model of Pelizaeus-Merzbacher disease. *Mol. Genet. Metab.* **106,** 108–114
25. Morimura, T., and Ogawa, M. (2009) Relative importance of the tyrosine phosphorylation sites of Disabled-1 to the transmission of Reelin signaling. *Brain Res.* **1304,** 26–37
26. Abematsu, M., Kagawa, T., Fukuda, S., Inoue, T., Takebayashi, H., Komiya, S., and Taga, T. (2006) Basic fibroblast growth factor endows dorsal telencephalic neural progenitors with the ability to differentiate into oligodendrocytes but not γ-aminobutyric acidergic neurons. *J. Neurosci. Res.* **83,** 731–743
27. Morimura, T., Hattori, M., Ogawa, M., and Mikoshiba, K. (2005) Disabled1 regulates the intracellular trafficking of reelin receptors. *J. Biol. Chem.* **280,** 16901–16908
28. Kaufman, R. J. (1999) Stress signaling from the lumen of the endoplasmic reticulum. Coordination of gene transcriptional and translational controls. *Genes Dev.* **13,** 1211–1233
29. Zhang, Y., Liu, R., Ni, M., Gill, P., and Lee, A. S. (2010) Cell surface relocalization of the endoplasmic reticulum chaperone and unfolded protein response regulator GRP78/BiP. *J. Biol. Chem.* **285,** 15065–15075
30. Suter, U., and Scherer, S. S. (2003) Disease mechanisms in inherited neuropathies. *Nat. Rev. Neurosci.* **4,** 714–726
31. Dickson, K. M., Bergeron, J. J., Shames, I., Colby, J., Nguyen, D. T., Chevet, E., Thomas, D. Y., and Snipes, G. J. (2002) Association of calnexin with mutant peripheral myelin protein-22 *ex vivo*. A basis for "gain-of-function" ER diseases. *Proc. Natl. Acad. Sci. U.S.A.* **99,** 9852–9857
32. Valentijn, L. J., Baas, F., Wolterman, R. A., Hoogendijk, J. E., van den Bosch, N. H., Zorn, I., Gabreëls-Festen, A. W., de Visser, M., and Bolhuis, P. A. (1992) Identical point mutations of PMP-22 in Trembler-J mouse and Charcot-Marie-Tooth disease type 1A. *Nat. Genet.* **2,** 288–291
33. Ionasescu, V. V., Searby, C. C., Ionasescu, R., Chatkupt, S., Patel, N., and Koenigsberger, R. (1997) Dejerine-Sottas neuropathy in mother and son with same point mutation of *PMP22* gene. *Muscle Nerve* **20,** 97–99
34. Suter, U., Moskow, J. J., Welcher, A. A., Snipes, G. J., Kosaras, B., Sidman, R. L., Buchberg, A. M., and Shooter, E. M. (1992) A leucine-to-proline mutation in the putative first transmembrane domain of the 22-kDa peripheral myelin protein in the trembler-J mouse. *Proc. Natl. Acad. Sci. U.S.A.* **89,** 4382–4386
35. Suter, U., Welcher, A. A., Ozcelik, T., Snipes, G. J., Kosaras, B., Francke, U., Billings-Gagliardi, S., Sidman, R. L., and Shooter, E. M. (1992) Trembler mouse carries a point mutation in a myelin gene. *Nature* **356,** 241–244
36. Zinszner, H., Kuroda, M., Wang, X., Batchvarova, N., Lightfoot, R. T., Remotti, H., Stevens, J. L., and Ron, D. (1998) CHOP is implicated in programmed cell death in response to impaired function of the endoplasmic reticulum. *Genes Dev.* **12,** 982–995
37. Sütterlin, C., Hsu, P., Mallabiabarrena, A., and Malhotra, V. (2002) Fragmentation and dispersal of the pericentriolar Golgi complex is required for entry into mitosis in mammalian cells. *Cell* **109,** 359–369
38. Lane, J. D., Lucocq, J., Pryde, J., Barr, F. A., Woodman, P. G., Allan, V. J., and Lowe, M. (2002) Caspase-mediated cleavage of the stacking protein GRASP65 is required for Golgi fragmentation during apoptosis. *J. Cell Biol.* **156,** 495–509
39. Lee, M. C., Miller, E. A., Goldberg, J., Orci, L., and Schekman, R. (2004) Bi-directional protein transport between the ER and Golgi. *Annu. Rev. Cell Dev. Biol.* **20,** 87–123
40. Marie, M., Sannerud, R., Avsnes Dale, H., and Saraste, J. (2008) Take the "A" train. On fast tracks to the cell surface. *Cell. Mol. Life Sci.* **65,** 2859–2874
41. Quarles, R. H. (2002) Myelin sheaths. Glycoproteins involved in their formation, maintenance and degeneration. *Cell. Mol. Life Sci.* **59,** 1851–1871
42. Munro, S., and Pelham, H. R. (1987) A C-terminal signal prevents secretion of luminal ER proteins. *Cell* **48,** 899–907
43. D'Souza-Schorey, C., and Chavrier, P. (2006) ARF proteins. Roles in membrane traffic and beyond. *Nat. Rev. Mol. Cell Biol.* **7,** 347–358
44. Griffiths, G., Ericsson, M., Krijnse-Locker, J., Nilsson, T., Goud, B., Söling, H. D., Tang, B. L., Wong, S. H., and Hong, W. (1994) Localization of the Lys, Asp, Glu, Leu tetrapeptide receptor to the Golgi complex and the intermediate compartment in mammalian cells. *J. Cell Biol.* **127,** 1557–1574
45. Ward, C. L., Omura, S., and Kopito, R. R. (1995) Degradation of CFTR by the ubiquitin-proteasome pathway. *Cell* **83,** 121–127
46. Shinde, V. M., Sizova, O. S., Lin, J. H., LaVail, M. M., and Gorbatyuk, M. S. (2012) ER stress in retinal degeneration in S334ter Rho rats. *PloS One* **7,** e33266
47. Higa, A., and Chevet, E. (2012) Redox signaling loops in the unfolded protein response. *Cell. Signal.* **24,** 1548–1555
48. Ellgaard, L., and Frickel, E. M. (2003) Calnexin, calreticulin, and ERp57. Teammates in glycoprotein folding. *Cell Biochem. Biophys.* **39,** 223–247
49. Bertolotti, A., Zhang, Y., Hendershot, L. M., Harding, H. P., and Ron, D. (2000) Dynamic interaction of BiP and ER stress transducers in the unfolded-protein response. *Nat. cell Biol.* **2,** 326–332
50. Yamamoto, K., Fujii, R., Toyofuku, Y., Saito, T., Koseki, H., Hsu, V. W., and Aoe, T. (2001) The KDEL receptor mediates a retrieval mechanism that contributes to quality control at the endoplasmic reticulum. *EMBO J.* **20,** 3082–3091
51. Anders, N., and Jürgens, G. (2008) Large ARF guanine nucleotide exchange factors in membrane trafficking. *Cell Mol. Life Sci.* **65,** 3433–3445
52. Citterio, C., Vichi, A., Pacheco-Rodriguez, G., Aponte, A. M., Moss, J., and Vaughan, M. (2008) Unfolded protein response and cell death after depletion of brefeldin A-inhibited guanine nucleotide-exchange protein GBF1. *Proc. Natl. Acad. Sci. U.S.A.* **105,** 2877–2882
53. Nakagomi, S., Barsoum, M. J., Bossy-Wetzel, E., Sütterlin, C., Malhotra, V., and Lipton, S. A. (2008) A Golgi fragmentation pathway in neurodegeneration. *Neurobiol. Dis.* **29,** 221–231

PLOS ONE

Gene Therapy Model of X-linked Severe Combined Immunodeficiency Using a Modified Foamy Virus Vector

Satoshi Horino[1,2], Toru Uchiyama[2], Takanori So[1], Hiroyuki Nagashima[1], Shu-lan Sun[1], Miki Sato[2], Atsuko Asao[1], Yoichi Haji[1], Yoji Sasahara[2], Fabio Candotti[3], Shigeru Tsuchiya[2], Shigeo Kure[2], Kazuo Sugamura[4], Naoto Ishii[1]*

1 Department of Microbiology and Immunology, Tohoku University Graduate School of Medicine, Sendai, Japan, **2** Department of Pediatrics, Tohoku University Graduate School of Medicine, Sendai, Japan, **3** Genetics and Molecular Biology Branch, National Human Genome Research Institute, National Institutes of Health, Bethesda, Maryland, United States of America, **4** Miyagi Cancer Center, Natori, Japan

Abstract

X-linked severe combined immunodeficiency (SCID-X1) is an inherited genetic immunodeficiency associated with mutations in the common cytokine receptor γ chain (γc) gene, and characterized by a complete defect of T and natural killer (NK) cells. Gene therapy for SCID-X1 using conventional retroviral (RV) vectors carrying the γc gene results in the successful reconstitution of T cell immunity. However, the high incidence of vector-mediated T cell leukemia, caused by vector insertion near or within cancer-related genes has been a serious problem. In this study, we established a gene therapy model of mouse SCID-X1 using a modified foamy virus (FV) vector expressing human γc. Analysis of vector integration in a human T cell line demonstrated that the FV vector integration sites were significantly less likely to be located within or near transcriptional start sites than RV vector integration sites. To evaluate the therapeutic efficacy, bone marrow cells from γc-knockout (γc-KO) mice were infected with the FV vector and transplanted into γc-KO mice. Transplantation of the FV-treated cells resulted in the successful reconstitution of functionally active T and B cells. These data suggest that FV vectors can be effective and may be safer than conventional RV vectors for gene therapy for SCID-X1.

Citation: Horino S, Uchiyama T, So T, Nagashima H, Sun S-l, et al. (2013) Gene Therapy Model of X-linked Severe Combined Immunodeficiency Using a Modified Foamy Virus Vector. PLoS ONE 8(8): e71594. doi:10.1371/journal.pone.0071594

Editor: Lishomwa C. Ndhlovu, University of Hawaii, United States of America

Received June 3, 2013; **Accepted** July 8, 2013; **Published** August 21, 2013

Funding: This study was supported in part by a grant-in-aid (#24659487 and #24390118) for scientific research on priority areas from the Ministry of Education, Science, Sports and Culture of Japan, a grant-in-aid for scientific research on priority areas from the Japan Society for the Promotion of Science, and grants (#111020001010004100) from the Japan Science and Technology Agency. The funders had no role in study design, data collection and analysis, decision to publish, or preparation of the manuscript. No additional external funding was received for this study.

Competing Interests: The authors have declared that no competing interests exist.

* E-mail: ishiin@med.tohoku.ac.jp

Introduction

X-linked severe combined immunodeficiency (SCID-X1) is a life-threatening immunodeficiency disorder, characterized by defective T and natural killer (NK) cell production and the development of functionally impaired B cells that lack the capacity to produce immunoglobulins. These defects result in a profound reduction in the development of both cellular and humoral immunity. SCID-X1 is caused by inactivating mutations in the gene encoding the cytokine receptor γ chain (γc), a common subunit of the receptors for interleukin (IL)-2, IL-4, IL-7, IL-9, IL-15, and IL-21 [1]. Bone marrow transplantation (BMT) from human leukocyte antigen (HLA)-identical siblings can cure the disease with a success rate of approximately 90%. However, BMT from non-HLA-identical donors results in lower survival rates due to a high risk for complications such as graft-versus-host disease, graft rejection, and incomplete T cell engraftment [2,3]. Consequently, gene therapy approaches have been developed as an alternative treatment option for those patients lacking appropriate donors.

The first gene therapy clinical trial for SCID-X1 was carried out by a French group in 1999 [4,5]. In that study, a conventional retroviral (RV) vector expressing γc was used, and resulted in the reconstitution of T and NK cell populations, and the recovery of humoral immunity. However, over time, acute T cell leukemia developed in 5 of the 20 patients receiving the therapy. The leukemia cells of these patients showed aberrant and high expressions of proto-oncogenes such as *LMO2*, which were caused by RV insertions within or near these loci [4,5]. To reduce the risk of vector-mediated insertional mutagenesis, various types of new vectors have since been developed [6,7].

Foamy virus (FV) is a non-pathogenic retrovirus belonging to the spumavirus genus and has unique biological characteristics, such as a wide host range (including humans), and wide tissue tropism [8,9]. Refined FV vectors that have large packaging capacities and are able to transduce murine and human hematopoietic stem cells (HSCs) have been reported [10–12]. In addition, FV vectors are reported to have a reduced tendency to integrate within or adjacent to the coding regions of genes compared to RV vectors. Due to these advantages, FV vectors have recently been used to correct genetic deficiencies in hematopoietic stem cells (HSCs) in several mouse models; these diseases include Wiskott–Aldrich syndrome (WAS) [13], leukocyte adhesion deficiency [14], Fanconi anemia [15], β-thalassemia [16], and X-linked chronic granulomatous disease [17].

In the present study, we evaluated the rate of insertional mutagenesis by a γc-FV vector compared to that of an RV vector in human T cells, and demonstrated the effectiveness of the γc-FV vector in a murine gene therapy model of SCID-X1.

Methods

All procedures were performed according to the protocols approved by the Institutional Committee for Use and Care of Laboratory Animals of Tohoku University, which was granted by Tohoku University Ethics Review Board (No. 2010MA165) and the Guide for Care and Use of Laboratory Animals published by the U.S. National Institutes of Health (NIH publication 85–23, revised 1996).

FV vector construction and production

FV vector plasmids were constructed as previously described [13,18,19]. In brief, a 631-bp *BspE*I and *Tth111*I restriction fragment from the ubiquitously acting chromatin-opening element promoter from the human HNRPA2B1-CBX3 locus (UCOE631) was isolated and inserted into the pΔΦ vector plasmid together with either the human γc (*IL2RG*) or enhanced green fluorescent protein (EGFP) complementary DNA (cDNA) to generate FV-IL2RG and FV-EGFP (Fig. 1A).

FV particles were produced by transfecting 293T cells with the resultant gene transfer vector plasmids and three helper plasmids (pCiGS, pCiPS, and pCiES) using FuGENE HD (Roche Applied Science), as previously described [13]. Culture supernatants were harvested after 48 hours and concentrated by ultracentrifugation.

A γc RV vector was constructed by inserting the human γc cDNA into the multi-cloning site of pMX-IRES-EGFP. Retroviral particles were produced by transfecting into amphotropic retrovirus packaging cells (PLAT-A cells) with pMx-IL2RG-IRES-EGFP using FuGENE HD. Culture supernatants containing the RV vector particles were harvested after 48 hours.

Cell lines

A human T cell line, ED40515(−) [20], which lacks γc expression, and an ED40515(−)-derived transfectant with a γc gene, EDγ, were described previously [21,22]. These cell lines were cultured in RPMI1640 medium supplemented with 10% FCS.

Mice

The γc-KO mice were previously reported [23]. γc-KO mice on a NOD/scid background [24] were obtained from the Central Institute for Experimental Animals (CIEA, Kawasaki, Japan). They were housed under specific pathogen-free conditions in individually ventilated cages and supplied with sterile food, water, and bedding. All procedures were performed according to protocols approved by the Institutional Committee for the Use and Care of Laboratory Animals of Tohoku University (2011MA139).

Vector transduction and BMT

Lineage marker depleted (Lin^-) cells were purified from the bone marrow cells of male γc-KO mice using magnetic cell sorting. The purified cells were exposed to FV vectors in StemSpan medium (StemCell Technologies Japan, Tokyo) supplemented with stem cell factor (50 ng/ml), IL-3 (5 ng/ml), Flt-3 ligand (5 ng/ml), and IL-6 (10 ng/ml) (all from Wako Pure Chemical Industries, Tokyo, Japan) on CH-296 (Retronectin; Takara Shuzo, Otsu, Japan)-coated plates for 16 hours. The transduced cells ($1–3\times10^6$) were then transplanted intravenously into 120 rad-irradiated female γc-KO mice on a NOD/scid background of 6–8 weeks of age. Eight to 12 weeks after BMT, and the peripheral blood cells and splenocytes were analyzed.

The ED40515 cell lines were similarly transduced with FV or RV vectors, except that cytokines were not added.

Immunofluorescence staining

For fluorescence-activated cell sorting (FACS) analysis, peripheral blood cells and splenocytes were collected from the mice. After removing erythrocytes with a lysing buffer, the cells were stained with anti-CD3-allophycocyanin (APC), anti-CD4-APC, anti-CD8-phycoerythrin (PE), anti-NK1.1-PE, anti-B220-APC, and/or anti-IgM-PE monoclonal antibodies (mAbs). Stained cells

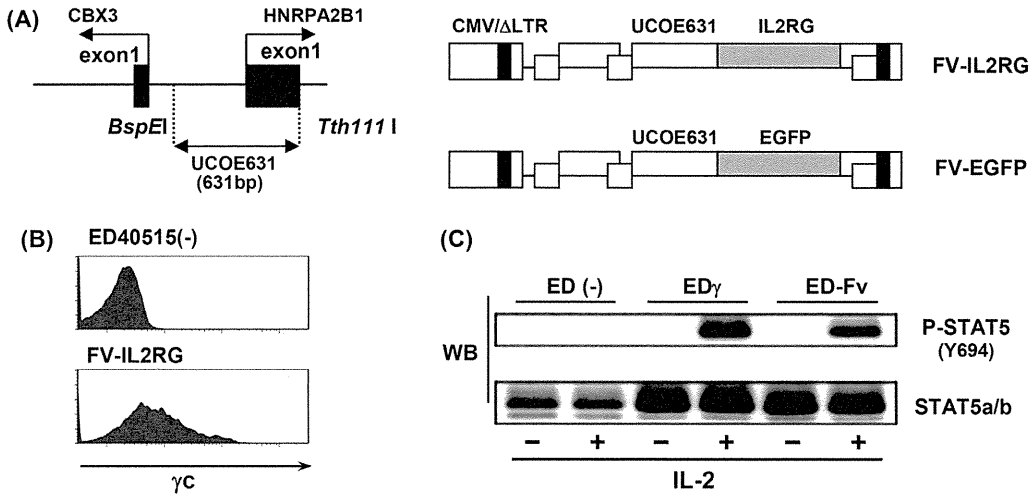

Figure 1. Structure and *in vitro* analysis of foamy virus vectors. (**A**) Structure of the foamy virus vectors. The UCOE631 promoter sequence from the human HNRPA2B1-CBX3 locus and transgenes were inserted into the FV vector. (**B**) Cell-surface expression of γc on ED40515(−) cells transduced with the FV-IL2RG vector. (**C**) STAT5 phosphorylation upon IL-2 stimulation. ED40515(−) cells, an ED40515(−)-derived transfectant with a γc gene, EDγ cells, and ED40515(−) cells transduced with the indicated vectors were stimulated with IL-2 for 30 min, and STAT5 phosphorylation in each cell line was detected by a STAT5 phosphospecific mAb.
doi:10.1371/journal.pone.0071594.g001

were analyzed with a FACS CantoII analyzer using the FACS Diva software (BD Biosciences, San Jose, CA).

Phosphorylated STAT5 detection

The IL-2-induced phosphorylation of STAT5 was detected by Western blotting as previously described [22]. In brief, cells were stimulated with 100 ng/ml IL-2 for 30 min at 37°C, collected, and lysed with a lysis buffer (20 mM Tris-HCl (pH 7.4), 150 mM NaCl, 2 mM EDTA, 1% NP-40, 50 mM NaF, 1 mM Na_3VO_4, and Protease Inhibitor Cocktail (Sigma-Aldrich Japan, Tokyo)). The protein lysates were separated by electrophoresis, transferred onto a polyvinylidene fluoride membrane, and blotted with STAT5 phosphospecific (pY694) antibodies (Cell Signaling Technology, Japan). Bound primary Abs were detected by a horseradish peroxidase-conjugated anti-rabbit IgG Ab followed by an enhanced chemiluminescence (ECL) detection reagent.

T cell proliferation and cytokine production

Spleen cells (1×10^5 cells/well) were stimulated with plate-coated anti-CD3 mAb (clone 2C11; 0.5 or 10 μg/ml) and/or 100 ng/ml recombinant human IL-2. T cell proliferation was measured after 48 hours by [^{3}H] thymidine incorporation and scintillation counting in triplicate. The stimulation index was calculated as the ratio of the incorporated radioactivity (cpm) of splenocytes from mice treated with FV-IL2RG-treated HSCs to that of splenocytes from mice treated with FV-EGFP-treated HSCs. IL-2 and IFN-γ production was assessed with an OptiEIA ELISA kit (BD Biosciences) after 24 hours and 72 hours, respectively, of stimulation, following the manufacturer's specifications.

Analysis of vector-insertion sites by ligation-mediated PCR

To determine the vector-integration sites, linker-mediated PCR was performed on genomic DNA isolated from γc-transduced ED40515(−) cells as previously described [13,25]. Briefly, the genomic DNA was digested with *Mse*I and *Pst*I, and the fragments were ligated to an MseI linker (5′-GTAATACGACTCACTA-TAGGGCTCCGCTTAAGGGACGAGGCGAATTCCCT-GAT-3′, 5′-PO4-TAGTCCCTTAAGCGGAG-NH2-3′). PCR was then performed with a linker-specific primer 5′-GTAATAC-GACTCACTATAGGGC-3′, and an FV long-terminal repeat-specific primer 5′-GTCTATGAGGAGCAGG AGTA-3′ or an RV long-terminal repeat-specific primer 5′-TAACCAAT-CAGTTCGCTTCTCGCTT-3′. A nested PCR was then performed using a linker-specific primer 5′-AGGGCTCCGCT-TAAGGGAC-3′, and an FV long-terminal repeat-specific primer 5′-CCTCCTTCCCTGTAATACTC-3′ or an RV long-terminal repeat-specific primer 5′-CTCAATAAAAGAGCCCA-CAACCCC-3′. The PCR products were subcloned into pCR2.1 using the TOPO cloning kit (Life Technologies Japan, Tokyo), and the vector/DNA junction sites were sequenced with an ABI 3100 Genetic Analyzer (Applied Biosystems). The recovered vector/DNA junctions were matched to the human genome using the BLAT software program and each insertion locus was identified. Since integration sites of conventional RV vectors are preferentially found within 15 kb of transcriptional start sites (TSS) [26,27], we calculated the percentages of all integration sites within 15 kb of TSS. The integration frequency was calculated as previously described [28]. In brief, FV vector integration sites were mapped relative to RefSeq gene transcription start sites, binned into different size sequence windows, and plotted as the percent of all integrations per kb. Genes within 30 kb of the integration sites were also compared to the list of annotated cancer genes in the Atlas of Genetics and Cytogenetics in the Oncology and Hematology database (http://atlasgeneticsoncology.org/).

Statistical analysis

Statistical analysis was performed using χ^2-test or Student's t-test. P-values <0.05 were considered significant.

Results

FV vector performance in human T cells

We constructed two FV vectors, FV-IL2RG and FV-EGFP, to express human γc and EGFP, respectively, both of which were driven by the ubiquitously acting chromatin-opening element promoter (Fig. 1A, and see Materials and Methods). This promoter consists of a methylation-free CpG island without classic enhancer activity. To evaluate the function of the FV-IL2RG vector-expressed γc chain, we infected ED40515(−), a human T cell line lacking γc [21,22], with the FV vectors. A flow cytometric analysis detected clear γc expression on the surface of the FV-IL2RG-treated cells (Fig. 1B). Western blot analysis showed the phosphorylation of Stat5 upon IL-2 stimulation, reflecting the activation of intracellular signaling through the vector-mediated γc (Fig. 1C), and indicating the expression of functional γc. These results indicated that FV vectors can effectively transfer and express the γc gene in human T cells.

Profile of provirus integration sites in human T cells

We identified 100 independent integration sites of the FV or RV provirus in ED40515(−) cells infected with each vector, using a standard linker-mediated PCR analysis. Fig. 2A shows that the frequency of integration sites located within gene transcriptional units was comparable between the FV (36%) and RV (42%) vectors. However, the FV integration sites showed a significantly lower likelihood (13%) of being located immediately up or downstream of transcriptional start sites than the RV integration sites (25%) (Fig. 2A). Furthermore, the FV integration sites in the human T cells showed only a modest preference for regions near transcriptional start sites compared to RV integration sites (Fig. 2B), consistent with the results of previous studies [13,25,29].

In addition, we examined the cancer-related genes located within 30 kb of the FV and RV integration sites because all the RV insertion sites in gene therapy-related leukemia were shown within gene or within 30 kb of TSS of LMO-2 or BMI1 [30]. One of the 100 FV integration sites was detected inside the cancer-related gene, TCF12, which is known as a negative regulator of cell proliferation, whereas three of the RV integration sites were detected within cancer-related genes, (Klf5, NUMB, and FHIT) all of which are known leukemia-related genes.

Collectively, these results suggest that FV vectors might have a lower risk of vector-mediated genotoxicity than conventional RV vectors.

In vivo assessment of T cell restoration after FV-mediated gene therapy

To evaluate the efficacy of FV vector-mediated γc expression *in vivo*, we performed BMT experiments. Bone marrow Lin$^-$ cells from γc-KO mice were transduced with FV-IL2RG or FV-EGFP vectors. The cellular transduction efficiency of both vectors was between 33 and 40%. The FV vector-infected cells were intravenously transplanted into γc-KO mice on a NOD/scid background. Since older γc-KO mice on a C57BL/6 background were found to contain CD3$^+$CD4$^+$ cells (data not shown), γc-KO

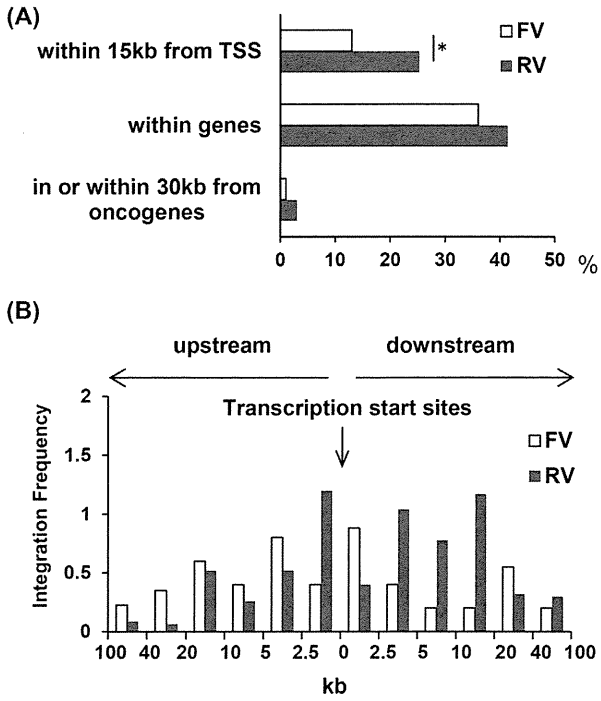

Figure 2. Profile of provirus integration in transduced cells. (**A**) Position of FV and RV integration sites. The percentage of all integration sites within 15 kb of transcriptional start sites, within genes that contain putative microRNA genes, and within 30 kb of oncogenes is shown for FV vector- or RV vector-treated cells. *$p<0.05$, χ^2-test. (**B**) A 100-kb window centered on TSS in the RefSeq database is shown. Relative frequencies of FV and RV vector integrations in each interval were calculated by dividing the percentage of integration b the indicated interval length.
doi:10.1371/journal.pone.0071594.g002

mice on a NOD/scid background were deemed a more suitable recipient for evaluating T cell reconstitution.

Eight weeks after transplantation, T cells emerged in the peripheral blood of the FV-IL2RG-treated group, and the clear expression of γc was confirmed on $CD8^+$ T cells (Fig. 3A). Gene therapy mice showed the recovery of CD4 and CD8 T cells as well as $B220^+$ IgM^+ B cells in spleen (in Figure 3B) although we could not detect NK cells. In addition, serum levels of IgM, IgG, and IgA were significantly elevated in FV-IL2RG-treated mice (Fig. 3C). These results indicate that HSCs transduced with FV-IL2RG have the potential for normal B and T cell differentiation.

We next investigated the functional capacity of the reconstituted T cells. Splenocytes from FV-IL2RG-treated mice showed proliferative responses following treatment with an anti-CD3 mAb, while those from the FV-EGFP-treated group did not (Fig. 4A). IL-2 stimulation induced proliferation through γc-transduced signals in T cells from FV-IL2RG-treated mice although stimulation with anti-CD3 mAb plus IL-2 did not enhance T cell proliferation compared to anti-CD3 mAb alone (Fig. 4A). The reconstituted T cells also produced IL-2 and IFN-γ upon stimulation with anti-CD3 mAb (Fig. 4B), indicating the functional restoration of T cells. Collectively, FV vector-mediated γc gene transfer was demonstrated to restore T and B cell differentiation and function *in vivo*.

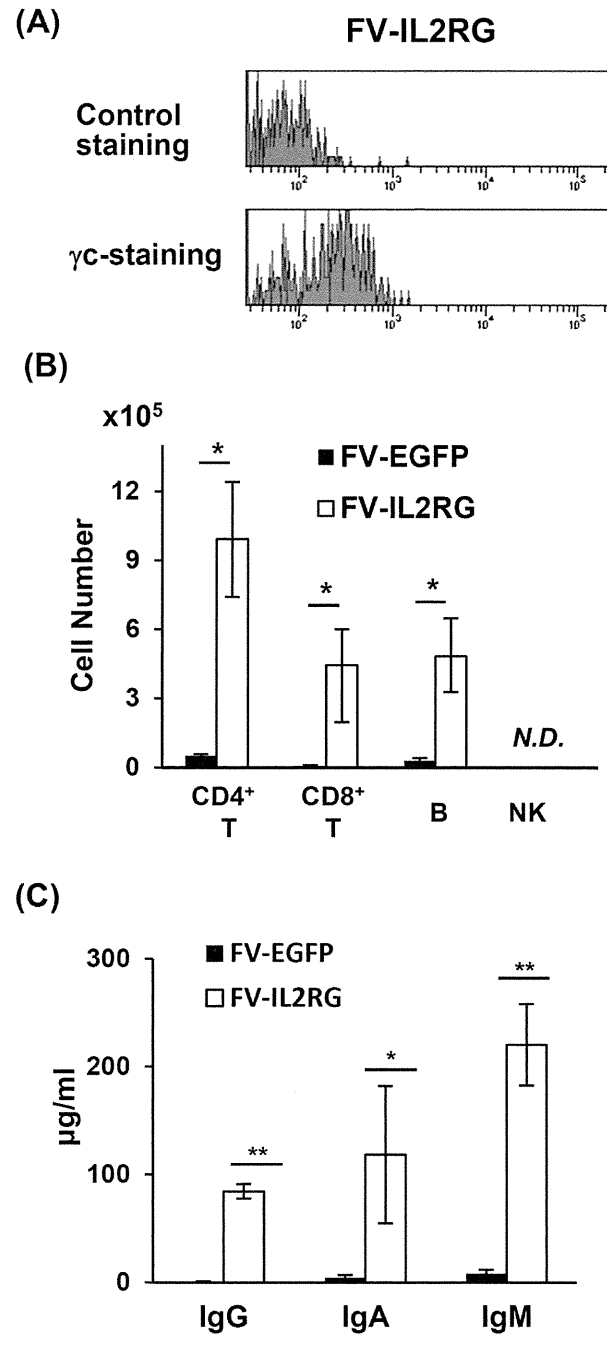

Figure 3. Reconstitution of T and B cells. (**A**) Cell-surface expression of γc on peripheral $CD8^+$ T cells in γc-KO mice treated with FV-IL2RG-treated HSCs. The upper and lower panels show isotype-control and γc-specific stainings, respectively. (**B**) The absolute numbers of $CD4^+$ T, $CD8^+$ T, $sIgM^+$ B, and NK cells in the spleen of γc-KO mice treated with FV-EGFP and FV-IL2RG (n = 4 in each group). *N.D.*, not detectable. (**C**) Serum IgM, IgG, and IgA in FV-IL2RG-treated mice. Serum levels of IgM, IgG, and IgA were measured by ELISA. Results shown are the mean ± SD of the stimulation index from 4 mice in each group. *$p<0.05$ and **$p<0.01$, Student t-test.
doi:10.1371/journal.pone.0071594.g003

Discussion

Vector-mediated insertional mutagenesis is a critical problem associated with conventional RV-mediated gene therapy treatments for SCID-X1. To address this issue, we developed a

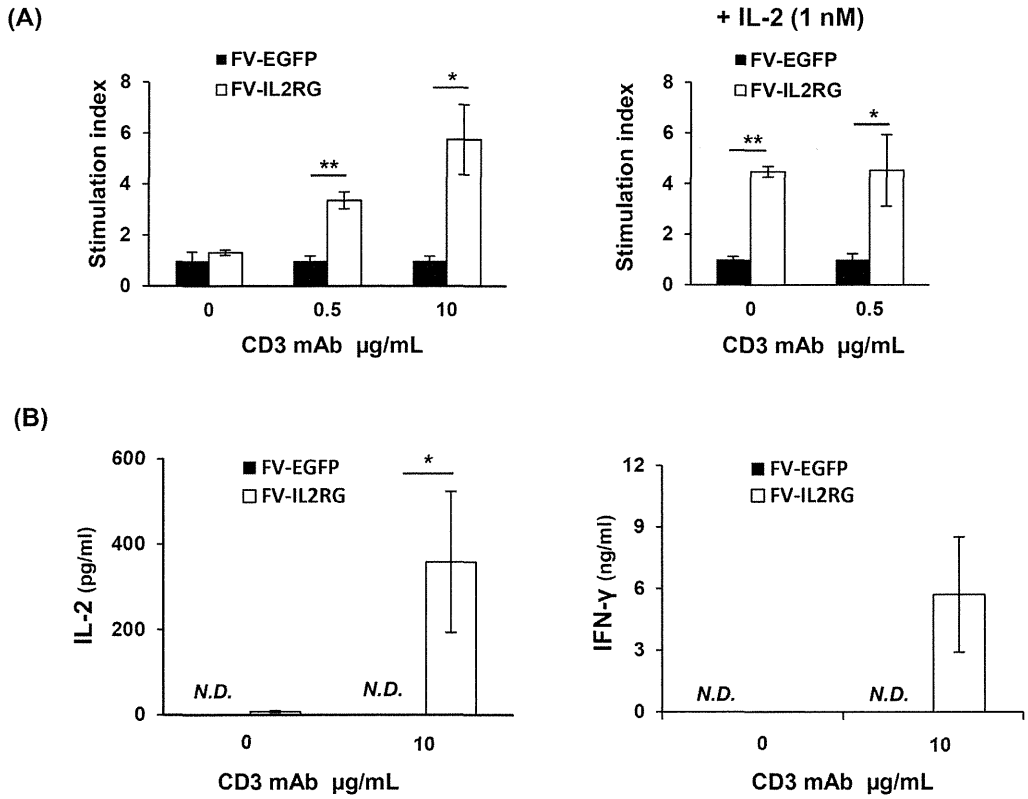

Figure 4. In vitro function of reconstituted T cells. (**A**) Splenocytes from recipient mice were stimulated with an anti-CD3 mAb at the indicated dose in the presence (right) or absence (left) of IL-2. Results shown are the mean ± SD of the stimulation index from 4 or 5 mice in each group. *p<0.05 and **p<0.01, Student t-test. (**B**) IL-2 and IFN-γ production by reconstituted T cells. Splenocytes from recipient mice were stimulated with an anti-CD3 mAb at the indicated dose. Culture supernatants were collected 24 and 72 hours after stimulation. Concentration of each cytokine in the supernatant was measured by ELISA. Results shown are the mean ± SD from 4 mice in each group. *p<0.05, Student t-test. *N.D.*, not detectable.
doi:10.1371/journal.pone.0071594.g004

modified FV vector carrying the human γc gene, and evaluated the vector-mediated insertional mutagenesis as well as the *in vivo* T, B, and NK cell reconstitution. Our findings demonstrated that the integration sites of the FV vector were significantly less likely to be located within or near transcriptional start sites compared to those of a conventional RV vector, suggesting that the FV vector had a lower risk for insertion-mediated genotoxicity. We also showed the successful reconstitution of functionally active T and B cells after the transplantation of HSCs containing a γc-FV vector into γc-KO recipient mice. This is the first reported use of an FV vector in a gene therapy mouse model of SCID-X1.

Previous studies showed that the use of classical RV vector for SCID-X1 gene therapy resulted in the development of leukemia in a number of patients [4,5]. The leukemogenesis associated with these vectors is likely to be due to inappropriate vector insertion in or near proto-oncogenes. Consistent with previous reports that FV vectors have a more random genomic integration pattern than RV vectors [28], our data indicated that the FV vector integration sites were less likely to be near transcription start sites than those of RV vectors (Fig. 2A, 2B). In addition, three integration sites of the RV vector were found within cancer-related genes (Klf5, NUMB, and FHIT), all of which are associated with leukemogenesis or leukemia progression [31–33]. Although one FV vector integration site was found within a cancer-related gene, TCF12, no evidence showing a relationship between TCF12 and leukemogenesis has been reported. These results are consistent with the accepted theory that FV is non-pathogenic for humans [8,9], and support the notion that FV vectors may be safer than conventional RV vectors.

The main objective of SCID-X1 gene therapy is the robust reconstitution of T, B, and NK cells. However, in the present study, use of the FV-IL2RG vector failed to reconstitute the NK cell population when monitored up to 4 months after gene therapy. One possible explanation for this deficiency may be that the human γc gene is not entirely compatible with the mouse system. Consistent with our findings, impaired NK cell reconstitution in mouse SCID-X1 gene therapy using the human γc gene was previously reported [34]; however, gene therapies in mouse models with RV vectors carrying the mouse γc gene were shown to reconstitute NK cells within two months [35–37]. NK cell development requires IL-15, while the differentiation and survival of T and B cells require IL-7. Receptors for both cytokines contain the shared γc subunit [1]. Therefore, the human γc might function less effectively as a mouse IL-15 receptor subunit than as a mouse IL-7 receptor subunit. In addition, T cell responses to IL-2 might also be insufficient as additional stimulation of IL-2 did not increase the T cell response with anti-CD3 mAb alone. Namely, the chimeric IL-2 and IL-15 receptors consisting of mouse α and β chains in combination with human γc might not fully function as a physiological mouse IL-2 and IL-15 receptors, respectively. In any case, the use of human γc, rather than the FV vector, is the probable cause of the impaired NK cell reconstitution and possible insufficient T cell function in this study.

We recently reported the successful treatment of a WAS mouse model using gene therapy with an FV vector [13]. Similar to

SCID-X1, the gene therapy for WAS requires T cell proliferative and functional restoration. Our studies collectively support the potential for modified FV vector-mediated gene therapy for the successful treatment of T cell immunodeficiencies. Moreover, FV vectors have also been shown to be effective for the treatment of red blood cell and granulocyte disorders in mouse models [14–17]. Based on their broad host range and ability to efficiently transduce HSCs, FV vectors may be applicable in gene therapies for many different hematopoietic disorders.

Over the last decade, novel modifications of RV vectors have been developed to overcome the problems associated with SCID-X1 gene therapy. However, it is still controversial which vector is the most favorable for safety. FV vectors have the potential to increase the efficacy of HSC-based gene therapies and to reduce the risk of genotoxicity. Although further studies are necessary, our data support the potential clinical application of FV vectors in gene therapy for SCID-X1 in the future.

Acknowledgments

We sincerely thank Drs. David W. Russell (University of Washington) and Adrian J. Thrasher (University College of London) for sharing reagents. We also thank the Biomedical Research Core Animal Pathology Platform for the essential technical support of pathological analysis.

Author Contributions

Conceived and designed the experiments: NI TU. Performed the experiments: SH TS HN SLS MS AA YH. Analyzed the data: ST SK KS. Contributed reagents/materials/analysis tools: TU YS FC. Wrote the paper: NI SH TU.

References

1. Sugamura K, Asao H, Kondo M, Tanaka N, Ishii N, et al. (1996) The interleukin-2 receptor gamma chain: its role in the multiple cytokine receptor complexes and T cell development in XSCID. Annu Rev Immunol 14: 179–205.
2. Buckley RH, Schiff SE, Schiff RI, Markert L, Williams LW, et al. (1999) Hematopoietic stem-cell transplantation for the treatment of severe combined immunodeficiency. N Engl J Med 340: 508–516.
3. Haddad E, Landais P, Friedrich W, Gerritsen B, Cavazzana-Calvo M, et al. (1998) Long-term immune reconstitution and outcome after HLA-nonidentical T-cell-depleted bone marrow transplantation for severe combined immunodeficiency: a European retrospective study of 116 patients. Blood 91: 3646–3653.
4. Fischer A, Hacein-Bey-Abina S, Cavazzana-Calvo M (2010) 20 years of gene therapy for SCID. Nat Immunol 11: 457–460.
5. Cavazzana-Calvo M, Fischer A (2007) Gene therapy for severe combined immunodeficiency: are we there yet? J Clin Invest 117: 1456–1465.
6. Montini E, Cesana D, Schmidt M, Sanvito F, Bartholomae CC, et al. (2009) The genotoxic potential of retroviral vectors is strongly modulated by vector design and integration site selection in a mouse model of HSC gene therapy. J Clin Invest 119: 964–975.
7. Modlich U, Navarro S, Zychlinski D, Maetzig T, Knoess S, et al. (2009) Insertional transformation of hematopoietic cells by self-inactivating lentiviral and gammaretroviral vectors. Mol Ther 17: 1919–1928.
8. Russell DW, Miller AD (1996) Foamy virus vectors. J Virol 70: 217–222.
9. Stirnnagel K, Luftenegger D, Stange A, Swiersy A, Mullers E, et al. (2010) Analysis of prototype foamy virus particle-host cell interaction with autofluorescent retroviral particles. Retrovirology 7: 45.
10. Vassilopoulos G, Trobridge G, Josephson NC, Russell DW (2001) Gene transfer into murine hematopoietic stem cells with helper-free foamy virus vectors. Blood 98: 604–609.
11. Josephson NC, Trobridge G, Russell DW (2004) Transduction of long-term and mobilized peripheral blood-derived NOD/SCID repopulating cells by foamy virus vectors. Hum Gene Ther 15: 87–92.
12. Leurs C, Jansen M, Pollok KE, Heinkelein M, Schmidt M, et al. (2003) Comparison of three retroviral vector systems for transduction of nonobese diabetic/severe combined immunodeficiency mice repopulating human CD34+ cord blood cells. Hum Gene Ther 14: 509–519.
13. Uchiyama T, Adriani M, Jagadeesh GJ, Paine A, Candotti F (2012) Foamy virus vector-mediated gene correction of a mouse model of Wiskott-Aldrich syndrome. Mol Ther 20: 1270–1279.
14. Bauer TR Jr, Allen JM, Hai M, Tuschong LM, Khan IF, et al. (2008) Successful treatment of canine leukocyte adhesion deficiency by foamy virus vectors. Nat Med 14: 93–97.
15. Si Y, Pulliam AC, Linka Y, Ciccone S, Leurs C, et al. (2008) Overnight transduction with foamyviral vectors restores the long-term repopulating activity of Fancc−/− stem cells. Blood 112: 4458–4465.
16. Morianos I, Siapati EK, Pongas G, Vassilopoulos G (2012) Comparative analysis of FV vectors with human alpha- or beta-globin gene regulatory elements for the correction of beta-thalassemia. Gene Ther 19: 303–311.
17. Chatziandreou I, Siapati EK, Vassilopoulos G (2011) Genetic correction of X-linked chronic granulomatous disease with novel foamy virus vectors. Exp Hematol 39: 643–652.
18. Trobridge G, Josephson N, Vassilopoulos G, Mac J, Russell DW (2002) Improved foamy virus vectors with minimal viral sequences. Mol Ther 6: 321–328.
19. Zhang F, Thornhill SI, Howe SJ, Ulaganathan M, Schambach A, et al. (2007) Lentiviral vectors containing an enhancer-less ubiquitously acting chromatin opening element (UCOE) provide highly reproducible and stable transgene expression in hematopoietic cells. Blood 110: 1448–1457.
20. Arima N, Kamio M, Imada K, Hori T, Hattori T, et al. (1992) Pseudo-high affinity interleukin 2 (IL-2) receptor lacks the third component that is essential for functional IL-2 binding and signaling. J Exp Med 176: 1265–1272.
21. Ishii N, Asao H, Kimura Y, Takeshita T, Nakamura M, et al. (1994) Impairment of ligand binding and growth signaling of mutant IL-2 receptor gamma-chains in patients with X-linked severe combined immunodeficiency. J Immunol 153: 1310–1317.
22. Asao H, Okuyama C, Kumaki S, Ishii N, Tsuchiya S, et al. (2001) Cutting edge: the common gamma-chain is an indispensable subunit of the IL-21 receptor complex. J Immunol 167: 1–5.
23. Ohbo K, Suda T, Hashiyama M, Mantani A, Ikebe M, et al. (1996) Modulation of hematopoiesis in mice with a truncated mutant of the interleukin-2 receptor gamma chain. Blood 87: 956–967.
24. Ito M, Hiramatsu H, Kobayashi K, Suzue K, Kawahata M, et al. (2002) NOD/SCID/gamma(c)(null) mouse: an excellent recipient mouse model for engraftment of human cells. Blood 100: 3175–3182.
25. Wu X, Li Y, Crise B, Burgess SM (2003) Transcription start regions in the human genome are favored targets for MLV integration. Science 300: 1749–1751.
26. Laufs S, Nagy KZ, Giordano FA, Hotz-Wagenblatt A, Zeller WJ, et al. (2004) Insertion of retroviral vectors in NOD/SCID repopulating human peripheral blood progenitor cells occurs preferentially in the vicinity of transcription start regions and in introns. Mol Ther 10: 874–881.
27. Montini E, Cesana D, Schmidt M, Sanvito F, Ponzoni M, et al. (2006) Hematopoietic stem cell gene transfer in a tumor-prone mouse model uncovers low genotoxicity of lentiviral vector integration. Nat Biotechnol 24: 687–696.
28. Trobridge GD, Miller DG, Jacobs MA, Allen JM, Kiem HP, et al. (2006) Foamy virus vector integration sites in normal human cells. Proc Natl Acad Sci U S A 103: 1498–1503.
29. Beard BC, Keyser KA, Trobridge GD, Peterson LJ, Miller DG, et al. (2007) Unique integration profiles in a canine model of long-term repopulating cells transduced with gammaretrovirus, lentivirus, or foamy virus. Hum Gene Ther 18: 423–434.
30. Hacein-Bey-Abina S, Garrigue A, Wang GP, Soulier J, Lim A, et al. (2008) Insertional oncogenesis in 4 patients after retrovirus-mediated gene therapy of SCID-X1. J Clin Invest 118: 3132–3142.
31. Zhu N, Gu L, Findley HW, Chen C, Dong JT, et al. (2006) KLF5 Interacts with p53 in regulating survivin expression in acute lymphoblastic leukemia. J Biol Chem 281: 14711–14718.
32. Ito T, Kwon HY, Zimdahl B, Congdon KL, Blum J, et al. (2010) Regulation of myeloid leukaemia by the cell-fate determinant Musashi. Nature 466: 765–768.
33. Stam RW, den Boer ML, Passier MM, Janka-Schaub GE, Sallan SE, et al. (2006) Silencing of the tumor suppressor gene FHIT is highly characteristic for MLL gene rearranged infant acute lymphoblastic leukemia. Leukemia 20: 264–271.
34. Huston MW, van Til NP, Visser TP, Arshad S, Brugman MH, et al. (2011) Correction of murine SCID-X1 by lentiviral gene therapy using a codon-optimized IL2RG gene and minimal pretransplant conditioning. Mol Ther 19: 1867–1877.
35. Otsu M, Sugamura K, Candotti F (2000) In vivo competitive studies between normal and common gamma chain-defective bone marrow cells: implications for gene therapy. Hum Gene Ther 11: 2051–2056.
36. Otsu M, Sugamura K, Candotti F (2001) Lack of dominant-negative effects of a truncated gamma(c) on retroviral-mediated gene correction of immunodeficient mice. Blood 97: 1618–1624.
37. Kume A, Koremoto M, Mizukami H, Okada T, Hanazono Y, et al. (2002) Selective growth advantage of wild-type lymphocytes in X-linked SCID recipients. Bone Marrow Transplant 30: 113–118.

T-cell receptor ligation causes Wiskott-Aldrich syndrome protein degradation and F-actin assembly downregulation

Yuko Watanabe, MD, PhD,[a]* Yoji Sasahara, MD, PhD,[a]* Narayanaswamy Ramesh, PhD,[b]* Michel J. Massaad, PhD,[b]* Chung Yeng Looi, PhD,[a] Satoru Kumaki, MD, PhD,[a] Shigeo Kure, MD, PhD,[a] Raif S. Geha, MD,[b]‡ and Shigeru Tsuchiya, MD, PhD[a]‡ *Miyagi, Japan, and Boston, Mass*

Background: Wiskott-Aldrich syndrome protein (WASP) links T-cell receptor (TCR) signaling to the actin cytoskeleton. WASP is normally protected from degradation by the Ca^{++}-dependent protease calpain and by the proteasome because of its interaction with the WASP-interacting protein.
Objective: We investigated whether WASP is degraded after TCR ligation and whether its degradation downregulates F-actin assembly caused by TCR ligation.
Methods: Primary T cells, Jurkat T cells, and transfected 293T cells were used in immunoprecipitation experiments. Intracellular F-actin content was measured in splenic T cells from wild-type, WASP-deficient, and c–Casitas B-lineage lymphoma (Cbl)-b–deficient mice by using flow cytometry. Calpeptin and MG-132 were used to inhibit calpain and the proteasome, respectively.
Results: A fraction of WASP in T cells was degraded by calpain and by the ubiquitin-proteasome pathway after TCR ligation. The Cbl-b and c-Cbl E3 ubiquitin ligases associated with WASP after TCR signaling and caused its ubiquitination. Inhibition of calpain and lack of Cbl-b resulted in a significantly more sustained increase in F-actin content after TCR ligation in wild-type T cells but not in WASP-deficient T cells.
Conclusion: TCR ligation causes WASP to be degraded by calpain and to be ubiquitinated by Cbl family E3 ligases, which targets it for destruction by the proteasome. WASP degradation might provide a mechanism for regulating WASP-dependent TCR-driven assembly of F-actin. (J Allergy Clin Immunol 2013;132:648-55.)

Key words: *Wiskott-Aldrich syndrome, Wiskott-Aldrich syndrome protein, T-cell receptor, calpain, ubiquitination, proteasome, F-actin, Cbl family proteins*

Abbreviations used
Arp: Actin-related protein
Cbl: Casitas B-lineage lymphoma
EVH1: Ena-VASP homology domain 1
IS: Immune synapse
TCR: T-cell receptor
WAS: Wiskott-Aldrich syndrome
WASP: Wiskott-Aldrich syndrome protein
WIP: WASP-interacting protein
WT: Wild-type
ZAP-70: ζ Chain–associated protein kinase of 70 kDa

Wiskott-Aldrich syndrome (WAS) is an X-linked recessive disorder characterized by variable immunodeficiency, eczema, and thrombocytopenia.[1] The gene for Wiskott-Aldrich syndrome protein (WASP) is mutated in patients with WAS and X-linked thrombocytopenia. *WAS* is located on Xp11.22-p11.23 and encodes a protein of 502 amino acids and approximately 60 kDa in molecular weight.[2,3] WASP expression is restricted to hematopoietic cells.[3]

WASP has an N-terminal Ena/VASP homology domain 1 (EVH1) domain, a Cdc42/Rac GTPase-binding domain, a proline-rich domain, a G actin–binding verprolin homology (V) domain, a cofilin homology (C) domain, and a C-terminal acidic (A) segment.[1] The last 3 domains are located at the C-terminal end of WASP and are collectively referred to as the VCA domain. WASP interacts with WASP-interacting protein (WIP) through its EVH1 domain; with Cdc42-GTP through its GTPase-binding domain; with multiple SH3 domain–containing proteins, which include Nck, Grb2, and cortactin, through its proline-rich region; and with the actin-related protein (Arp) 2/3 complex that initiates actin polymerization through its VCA domain.[4-6]

WASP plays a critical role in T-cell activation and actin reorganization.[7-9] T cells from patients with WAS and $WASP^{-/-}$ mice are deficient in their ability to increase their F-actin content, secrete IL-2, and proliferate after T-cell receptor (TCR) ligation.[10-12] WASP exists in cells in a closed inactive conformation through intramolecular interactions that prevent the VCA domain from activating the Arp2/3 complex. Binding of Cdc42-GTP or of the SH3 domain of adaptor proteins, as well as phosphorylation of tyrosine (Y) at position 291, is thought to cause a conformational change in WASP, which allows the VCA domain to interact with and activate the Arp2/3 complex.[5,13-15] The WASP-interacting protein (WIP) is expressed at high levels in lymphoid tissues. Most of WASP is associated with WIP in T cells.[16] WIP binds through its C-terminal end to the EVH1 domain of WASP. WIP plays an important role in the recruitment of the WASP-WIP complex to ζ chain–associated protein kinase of 70 kDa (ZAP-70) and

From [a]the Department of Pediatrics, Tohoku University Graduate School of Medicine, Miyagi, and [b]the Division of Immunology, Children's Hospital, and the Department of Pediatrics, Harvard Medical School, Boston.
*These authors contributed equally to this work.
‡These authors contributed equally as senior authors.
Supported by grants-in-aid from the Japan Ministry of Education, Culture, Sports, Science and Technology and a grant for research on intractable diseases from the Japan Ministry of Health, Labour and Welfare (to Y.S. and S.T.), grants from the Japan Foundation for Pediatric Research and the Mother and Child Health Foundation (to Y.S.) and by US Public Health Service grant HL059561.
Disclosure of potential conflict of interest: The authors have been supported by one or more grants from the National Institutes of Health.
Received for publication January 9, 2013; revised March 28, 2013; accepted for publication March 29, 2013.
Available online May 16, 2013.
Corresponding author: Yoji Sasahara, MD, PhD, Department of Pediatrics, Tohoku University Graduate School of Medicine, 1-1 Seiryo-machi, Aoba-ku, Sendai, Miyagi 980-8574, Japan. E-mail: ysasahara@med.tohoku.ac.jp.
0091-6749/$36.00

http://dx.doi.org/10.1016/j.jaci.2013.03.046

to the immunologic synapse after TCR ligation.[17] More importantly, WIP stabilizes WASP in T cells. This is evidenced by the finding that WASP levels are significantly reduced in T cells from $WIP^{-/-}$ mice and a WIP-deficient patient.[16,18] Furthermore, most missense mutations in WASP that result in diminished WASP levels are localized to the WIP-binding EVH1 domain of WASP and disrupt the WASP-WIP interaction.[19,20] Expression of the WASP-binding domain of WIP in these cells restores WASP levels close to normal.[21] Treatment with calpain and proteasome inhibitors increases WASP protein levels in T cells from $WIP^{-/-}$ mice and patients with WAS with missense mutations that disrupt WIP binding,[16] indicating that WASP can be subject to degradation by calpain and the ubiquitin-proteasome pathway.

Unregulated activation of WASP is detrimental to many cell types, especially cells of the myeloid lineage. Three different mutations of WASP, namely L270P, S272P, and I294T, destroy the autoinhibitory conformation of WASP, resulting in a constitutively active protein, and cause X-linked neutropenia.[22] The L270P and S272P mutations localize to the GTPase-binding domain,[23] whereas the I294T mutation is located close to the tyrosine residue Y291, which, when phosphorylated, results in the activation of WASP.[24] Knock-in mouse models mimicking the L270P and I294T mutations have been described.[25] T and B cells from these mice show a marked increase in F-actin levels but migrate normally in response to chemokines.

In this study we demonstrate that TCR ligation causes WASP to be degraded by calpain and by Casitas B-lineage lymphoma (Cbl)–mediated ubiquitination and proteasomal destruction. We demonstrate that WASP degradation provides a mechanism for downregulating TCR-driven assembly of F-actin.

METHODS

Cell lines and T cells

Jurkat T cells were obtained from the American Type Culture Collection and maintained in RPMI medium (Gibco, Carlsbad, Calif) supplemented with 10% FBS. 293T cells were a gift from Dr N. Ishii (Tohoku University, Sendai, Japan) and were maintained in Dulbecco modified Eagle medium (Gibco) supplemented with 10% FBS. Spleens from Cbl-b knockout (*Cbl-b*$^{-/-}$) mice and genetically matched wild-type (WT) shipping controls were a generous gift from Dr H. Gu, Columbia University. WASP-deficient mice were obtained from Dr Scott Snapper. Splenic T cells were isolated by using T-cell enrichment columns (Miltenyi Biotec, Bergisch Gladbach, Germany).

Antibodies

Anti-WASP 5A5 mAb, which recognizes the epitope in the region corresponding to amino acids 146 to 265, was developed in our laboratory.[26] Anti-WASP rabbit polyclonal antibody K374 (a gift from Dr Ignacio Molina) is directed to the C-terminal 20 amino acids of WASP.[16] Anti–phospho-WASP antibody, which recognized WASP phosphorylated on Y291, was purchased from Abcam (Cambridge, United Kingdom). Anti-ubiquitin mAb P4D1, anti–c-Cbl mAb A-9, and anti–Cbl-b mAb G-1 were from Santa Cruz Biotechnology (Santa Cruz, Calif). Anti-actin mAb and anti-FLAG mAb were from Sigma (St Louis, Mo). Anti-HA mAb was from Cell signaling (Danvers, Mass). Control rabbit IgG was from Upstate (Billerica, Mass).

TCR stimulation, immunoprecipitation, and Western blotting

TCR ligation was performed, as described previously.[17] Briefly, T cells were incubated with 10 μg/mL anti-CD3 mAb UCHT1 (Calbiochem, San Diego, Calif) on ice for 20 minutes, followed by cross-linking with 15 μg/mL goat anti-mouse IgG (H+L; Caltag, Buckingham, United Kingdom) at 37°C for the indicated period. Cells were lysed in ice-cold lysis buffer containing 1% Triton X-100 and protease inhibitors. Cell lysates were clarified at 14,000*g* for 20 minutes at 4°C. For immunoprecipitation, cell lysates were precleared with protein G–Sepharose (GE Healthcare, Fairfield, Conn) for 2 hours and incubated overnight at 4°C with 4 μg of the indicated antibody preadsorbed onto protein G–Sepharose. Beads were washed 4 times with modified lysis buffer containing 0.2% Triton X-100. Bound proteins were eluted, run on 10% SDS-PAGE gels, and analyzed by means of Western blotting with the indicated antibodies followed by anti-mouse or anti-rabbit antibodies conjugated to horseradish peroxidase and enhanced chemiluminescent detection (Amersham Life Sciences, Piscataway, NJ). Densitometry was performed with CS Analyzer version 2.08 software (ATTO Corporation, Tokyo, Japan) or ImageJ version 1.45 software.

Calpain and proteasome inhibition

The proteasome inhibitor MG132 and the calpain inhibitor calpeptin were purchased from Calbiochem. Cells were cultured with calpeptin (1 μmol/L) or MG132 (10 μmol/L) for 6 hours before anti-CD3 stimulation.

Expression vectors and transfection

Human pcDNA3.1-EGFP-hWASP-WT was a generous gift from Dr K. A. Siminovitch (University of Toronto, Toronto, Ontario, Canada). Control pAcGFP1-C1 vector was purchased from Clontech (Mountain View, Calif). Human pcDNA3.1-3xFLAG-c-Cbl-WT, pcDNA3.1-3xFLAG-Cbl-b-WT, and pcDNA3.1-HA-Ub were gifts from Drs N. Ishii and Y. Tanaka (Tohoku University).[27] Control p3xFLAG-CMV-14 vector was purchased from Sigma. 293T cells were transiently transfected with lipofectamine, as described previously,[27] and harvested 48 hours after transfection.

Determination of cellular F-actin content

Flow cytometric analysis of F-actin content was performed, as described previously.[16] Briefly, mouse T cells were purified by using negative selection with the Pan T Cell Isolation Kit (Miltenyi Biotec) and then incubated for 6 hours with 1 μmol/L calpeptin. Cells were then washed and incubated with 10 μg/mL rat anti-mouse CD3 mAb (Serotec, Oxford, United Kingdom) for 30 minutes on ice. Cells were stimulated for the indicated times by cross-linking with goat anti-rat IgG (H+L) secondary antibody (Jackson Immunoresearch, West Grove, Pa). Cells were fixed in 4% formaldehyde, washed, and permeabilized with the CytoFix/CytoPerm cell staining kit (BD Biosciences, San Jose, Calif). F-actin was stained with tetramethylrhodamine isothiocyanate–labeled phalloidin (Invitrogen, Carlsbad, Calif). F-actin content was analyzed by measuring the mean fluorescent intensity with FACS LSRFortessa (Becton Dickinson) and FlowJo (TreeStar, Ashland, Ore) software.

Statistical analysis

Statistical analysis was performed with the Student *t* test.

RESULTS

WASP is C-terminally truncated by calpain after TCR ligation

Purified peripheral blood T cells were stimulated with anti-CD3 mAb followed by cross-linking with secondary antibody and cell lysates were immunoblotted for WASP to investigate whether WASP is degraded after TCR ligation. Immunoblotting with mAb 5A5, which recognizes an epitope in the region corresponding to amino acids 146 to 265, revealed a 62- to 64-kDa band in unstimulated T cells (Fig 1, *A*), as previously observed.[28] Stimulation with anti-CD3 resulted in the appearance of a 55-kDa

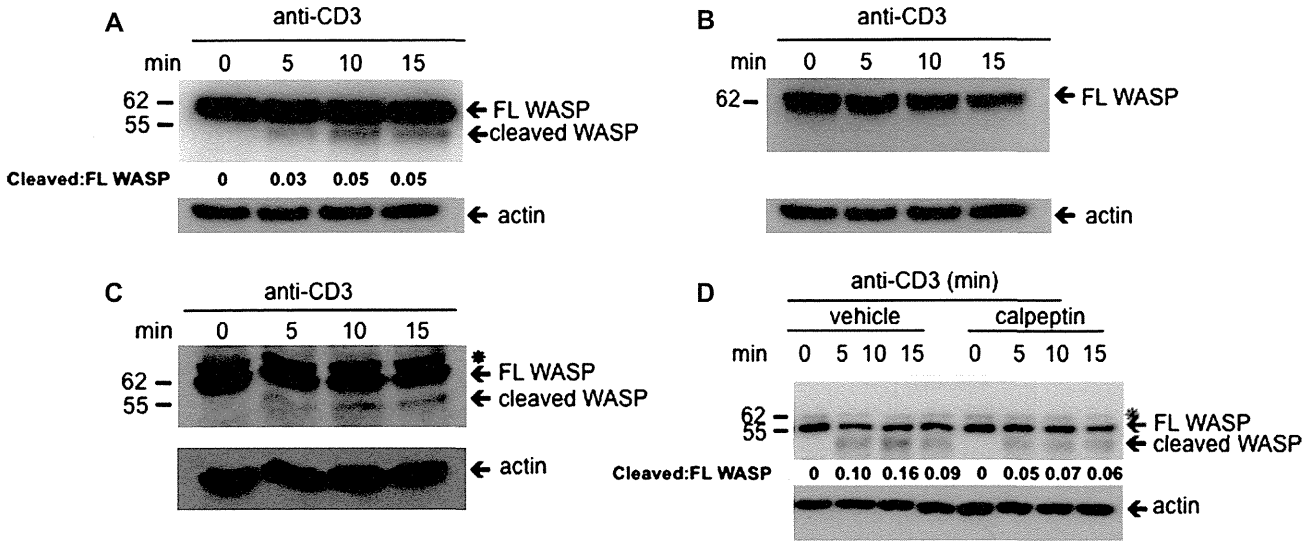

FIG 1. WASP is cleaved by calpain after TCR ligation. **A** and **B,** WASP immunoblot of peripheral blood T cells stimulated for 0 to 15 minutes with anti-CD3 mAb using mAb 5A5 (Fig 1, *A*) or polyclonal antibody K374 (Fig 1, *B*). **C,** WASP immunoblot of Jurkat T cells stimulated with anti-CD3 mAb using mAb 5A5. **D,** Effect of pretreatment for 6 hours with calpeptin on anti-CD3–driven WASP degradation in peripheral blood T cells. Lysates were immunoblotted with mAb 5A5. *Nonspecific band. The positions of molecular weight markers are indicated on the *left* in Fig 1, *A* to *D*. The ratio of cleaved WASP to full-length *(FL)* WASP in Fig 1, *A* and *D*, represents the mean of 5 experiments. Similar results were obtained in Fig 1, *A* to *D*, in 5 independent experiments.

WASP fragment at 5 minutes, which increased at 10 and 15 minutes after stimulation. Scanning densitometric analysis revealed that the intensity of the cleaved WASP band was approximately 5% that of the full-length WASP band at 10 and 15 minutes after stimulation. Similar results were obtained in Jurkat T cells (Fig 1, *C*).

Immunoblotting lysates of T cells with the rabbit polyclonal antibody K374 raised against the C-terminal 20 amino acids of WASP revealed the same 62- to 64-kDa band detected by using mAb 5A5 but did not detect the 55-kDa WASP fragment in anti-CD3–stimulated T cells that was detected by using mAb 5A5 (Fig 1, *B*). Similar results were obtained in Jurkat T cells (data not shown). This result indicates that the 55-kDa WASP fragment lacks the C-terminal VCA domains of WASP (amino acids 421-502) responsible for its actin-polymerizing activity.

Calpain cleaves WASP *in vitro*[29] and contributes to WASP degradation in WIP-deficient T cells.[16,30] To examine whether calpain was responsible for the cleavage of WASP after TCR ligation, T cells were pretreated with the calpain inhibitor calpeptin for 6 hours, washed, and stimulated with anti-CD3 mAb for 5 minutes. Preincubation with calpeptin attenuated by approximately 50% the generation of the 55-kDa WASP fragment in response to anti-CD3 stimulation (Fig 1, *D*), strongly suggesting that calpain mediates the C-terminal truncation of WASP after TCR/CD3 ligation, at least in part.

WASP is ubiquitinated and degraded by the proteasome in T cells after TCR ligation

In the absence of WIP, WASP is degraded by the ubiquitin-proteasome pathway.[16,30] To investigate whether WASP is a substrate for ubiquitination, we incubated *in vitro* transcribed and translated WASP with purified ubiquitin and ubiquitin-conjugating enzymes (mixture of E1, E2, and E3 enzymes), and the reaction mixture was immunoblotted with anti-ubiquitin mAb. WASP was polyubiquitinated in the presence of ubiquitin and ubiquitin-conjugating enzymes, as indicated by an intense high-molecular-weight smear (Fig 2, *A*). Addition of the 26S proteasome fraction to the ubiquitination mixture resulted in marked attenuation of the ubiquitinated WASP smear. These results indicate that after TCR/CD3 ligation, WASP is subject to ubiquitination, which targets it for destruction by the proteasome.

We next examined whether WASP is ubiquitinated in T cells after TCR ligation. Fig 2, *B*, shows the appearance of polyubiquitinated WASP after anti-CD3 mAb stimulation of Jurkat T cells. To examine whether WASP ubiquitinated after TCR ligation is targeted for destruction by the proteasome, Jurkat T cells were pretreated with the proteasome inhibitor MG132 for 6 hours and then stimulated with anti-CD3 mAb for 10 minutes, and WASP immunoprecipitates were prepared from their lysates and probed for ubiquitin. Fig 2, *C*, shows that ubiquitinated WASP was weakly detectable in unstimulated Jurkat cells, but its levels increased after TCR/CD3 stimulation. Pretreatment with MG132 modestly increased the amounts of ubiquitinated WASP in unstimulated Jurkat cells and strongly increased the amounts of ubiquitinated WASP detected after TCR/CD3 ligation. These results indicate that WASP is ubiquitinated and degraded by the proteasome after TCR ligation.

The Cbl family proteins c-Cbl and Cbl-b associate with WASP after TCR ligation and act as E3 ubiquitin ligases for WASP

Members of the Cbl family of E3 ubiquitin ligases are negative regulators in TCR signaling.[31,32] We tested the hypothesis that Cbl proteins might be involved in WASP ubiquitination. We first